Performance Degradation Due to Micro Fouling Layers in Large-Scale Industrial Heat Exchangers

A Thesis Presented for the
Master of Science
Degree
The University of Tennessee, Knoxville

Derrick Alan Talley
August 2019

Copyright © 2019 by Derrick Alan Talley
All rights reserved.

ACKNOWLEDGEMENTS

I would like to first thank my wife for her continuous encouragement, for her patience, and for being a relentless source of motivation as I completed this thesis and my graduate studies. Next, I would like to thank my committee chair, Dr. Feng-Yuan Zhang, for his mentorship and support during my time at UTSI. Also, thank you to my committee members, Dr. Steve Books and Dr. Reza Abedi, for their review and advice for my research. In addition, I thank my NANOHELP research partners for welcoming me to the group, providing me the opportunity to learn about their various research topics, and providing crucial assistance as I completed my research. Lastly, I would like to thank my coworkers at AEDC for their mentorship as I started my career and assistance as I studied the K1 Cooler and completed this thesis.

This work completed herein was completed at Arnold Engineering Development Complex. This report was released on May 23, 2019 per PA# AEDC2019-100 with the following distribution statement: Distribution Statement A – Approved for Public Release.

ABSTRACT

The 16T Propulsion Wind Tunnel, located at Arnold Engineering Development Complex (AEDC), Arnold Air Force Base, Tennessee, is a closed-circuit wind tunnel consisting of a 16-foot by 40-foot long test section. The test section temperature is controlled by a 50-foot diameter cross flow air to water heat exchanger, the K1 Cooler. Over the last several years, the performance of the K1 Cooler has deteriorated and the thermal capacity of the cooler has come into question. A study was initiated to quantify the deterioration and determine how critical bundle replacement was to future operations.

To aid this investigation, multiple tubes were removed from the cooler and analyzed. It was found that the tubes had an internal layer of particulate fouling that could be causing a degradation in cooler performance. Since the original design did not account for an accumulating internal fouling layer, a Matlab model was created to simulate cooler exit air and water temperatures for varying values of the fouling layer thermal conductivity and fouling layer thickness. Results were compared to empirical data at multiple test conditions.

TABLE OF CONTENTS

Chapter One Introduction and General Information 10
Introduction to the PWT K1 Cooler 10
Problem Statement 14
Chapter Two Literature Review 15
Heat Exchanger Design 15
Fouling in Heat Exchangers 15
Particulate Fouling 15
Fouling Process 16
Quantifying Fouling Accumulation 20
Fouling Resistance Calculations 22
Chapter Three Materials and Methods 24
Instrumentation of K1 Cooler 24
Fouling Layer Investigation 27
Fouling Layer Thickness Measurements 27
Fouling Layer Composition 31
Cooler Bundle Analysis 32
Model of Cooler Bundle 32
General Assumptions 35
16T Airside Parameter Locations 36
Convection Heat Transfer Analysis 37
Chapter Four Results and Discussion 45
Fouling Layer Thermal Conductivity Analysis 45
Fouling Layer Thickness Analysis 49
Source of Potential Error 52
Chapter Five Conclusions and Recommendations 53
List of References 56
Vita 58

LIST OF TABLES

Table 3.1: Sample Tube Thickness 30
Table 3.2: Fouling Layer Composition (%) 31
Table 4.1: 16T Test Conditions 45
Table 4.2: Calculated Thermal Conductivity for Each Test 48
Table 4.3: Design Envelope for K1 Cooler 49
Table 5.1: Fouling Resistance 54
Table 5.2: Comparison between New Bundle and Current Bundle 54

LIST OF FIGURES

Figure 1.1: K1 Cooler 10
Figure 1.2: Section View of K1 Cooler 11
Figure 1.3: K1 Cooler Bundles 12
Figure 1.4: Section View of K1 Cooler Bundles 12
Figure 1.5: View of Bundle from Inside the Fairings 13
Figure 1.6: View of Bundle from Inside the Fairings 13
Figure 2.1: Typical Fouling Process [Awad, 2011] 17
Figure 2.2: Typical Fouling Curves [Kazi, 2012] 17
Figure 2.3: Forces Acting on Fouling Particle [Razmavar, 2016] 19
Figure 2.4: Typical Fouling Layer Accumulation Curve [Kazi, 2012] 21
Figure 3.1: Downstream RTDs 25
Figure 3.2: Typical RTD location for Levels 1 and 6 (left) and Levels 2-5 (right) 25
Figure 3.3: Upstream RTDs – Air Side 26
Figure 3.4: K1 Cooler Sump Pit – Location of Discharge RTD 26
Figure 3.5: Internal Surface of Tube 27
Figure 3.6: Magnified View of Tube Surface 28
Figure 3.7: Plan view of Fouling Layer 28
Figure 3.8: Section View 29
Figure 3.9: Zoom-in Section View 29
Figure 3.10: K1 Cooler Tube 32
Figure 3.11: Typical Cross Section View of Tube 33
Figure 3.12: Typical Cooler Bundle Tube 33
Figure 3.13: Side View of Cooler Bundle Tube 34
Figure 3.14: 141 µm Fouling Layer 34
Figure 3.15: 500 µm Fouling Layer 35
Figure 3.16: Illustration of 16T Airside Parameter Location 36
Figure 3.17: Schematic of Bundle Arrangement 41
Figure 4.1: Exit Air Temperature for Varying Thermal Conductivity 46
Figure 4.2: Exit Water Temperature for Varying Thermal Conductivity 46
Figure 4.3: Heat Transfer for Varying Thermal Conductivity 47
Figure 4.4: Heat Transfer for Varying Fouling Layer Thickness 50
Figure 4.5: Exit Air Temperature for Varying Fouling Layer Thickness 50
Figure 4.6: Air Temperature across Bundle for Varying Fouling Layer Thickness 51
Figure 4.7: Exit Water Temperature for Varying Fouling Layer Thickness 51
Figure 4.8: Water Temperature across Bundle for Varying Fouling Layer Thickness 52

NOMENCLATURE

A_{fin} – Surface Area of Fin [m^2]
A_{tube} – Outside Surface Area of Tube [m^2]
A_i – Total Surface of Inside of Tube [m^2]
$A_{i,cs}$ – Inside Cross-Sectional Area of Tube [m^2]
A_n – Cross Sectional Area [m^2]
A_o – Total Surface Area of Cooler Bundle [m^2]
A^* – Choked Flow Area [m^2]
C – Constant [K]
c_p – Specific Heat at Constant Pressure [$J/kg \cdot K$]
d_{fin} – Outside Diameter of Fin [mm]
d_{foul} – Inner diameter of Fouling Layer [mm]
d_i – Inside Diameter of Tube [mm]
d_o – Outside Diameter of Tube [mm]
h - Convective Heat Transfer Coefficient [$W/m^2 \cdot K$]
h – Enthalpy [J]
h_t – Stagnation or Total Enthalpy [J]
k – Thermal Conductivity [$W/m \cdot K$]
l – Fin Height [mm]
L_{tube} – Length of Tube (one pass) [m]
$L_{tube,total}$ – Total length of Tube Length per Bundle [m]
M_n – Mach Number
m_f – Accumulated Mass of Fouling Material per Unit Area [kg/m^2]
m_f^* - Asymptotic value of m_f [kg/m^2]
$\dot{m}_n$ – Mass Flow Rate [kg/s]
$\dot{m}_d$ – Fouling Deposition Rate [kg/s]
$\dot{m}_r$ - Fouling Removal Rate [kg/s]
N_{bundle} – Number of Bundle in K1 Cooler
N_{fin} – Number of Fin per Tube
N_{pass} – Number of Passes per Tube
N_{tube} – Number of Tubes per Bundle
$\overline{Nu}$ – Average Nusselt Number
P_n – Static Pressure [Pa]
P_{tn} – Stagnation or Total Pressure [Pa]
Pr – Prandtl Number
Q – Convective Heat Transfer [W]
R – Ideal Gas Constant [$J/kg \cdot K$]

R_f – Fouling resistance $[m^2 \cdot K/W]$
R_f^* - Asymptotic value of R_f $[m^2 \cdot K/W]$
Re – Reynolds Number
s – Distance between fins [mm]
t – Time [s]
t_c – Average Residence Time [s]
T_n – Static Temperature [K]
T_{tn} – Stagnation or Total Temperature [K]
U – Overall Heat Transfer Coefficient $[W/m^2 \cdot K]$
U_c – Overall Heat Transfer Coefficient of Clean Heat Exchanger $[W/m^2 \cdot K]$
U_f – Overall Heat Transfer Coefficient of Fouled Heat Exchanger $[W/m^2 \cdot K]$
V_n – Velocity $[m/s]$
x_n or δ_n – Thickness [mm or μm]
X_L – Lateral Distance between Tubes [mm]
X_T – Transverse Distance between Tubes [mm]
$\beta = 1/t_c$ $[s^{-1}]$
γ – Specific Heat Ratio
ΔT_{LM} – Log Mean Temperature Difference [K]
ρ_n – Density $[kg/m^3]$
μ – Viscosity [μPa·s]
Φ_d – Fouling Deposition Rate $[m^2 \cdot K/W]$
Φ_r – Fouling Removal Rate $[m^2 \cdot K/W]$

Variables identified with an *n* subscript above are used on multiple occasions. The following identifiers apply:

1, 2, 3, 4, 5 – Airside Locations (Figure 3.15)
a – Air
f or $foul$ – Fouling Layer/Material
fin – K1 Cooler Bundle Fins
w – Water
wi – K1 Water In
wo – K1 Water Out

CHAPTER ONE
INTRODUCTION AND GENERAL INFORMATION

Introduction to the PWT K1 Cooler

The Propulsion Wind Tunnel Facility (PWT), located at AEDC on Arnold Air Force Base, TN, was designed and constructed in the 1950s. The facility consists of three wind tunnels: the 16-foot transonic (16T), the 16-foot supersonic (16S), and the 4-foot transonic (4T). 16T is a transonic tunnel with operating Mach numbers from 0.06 to 1.6 [Test Facilities Handbook, 1992]. The airflow is generated by one three-stage axial compressor. The K1 Cooler is required to remove the heat of compression and set tunnel temperature. Standard operation occurs with a test section total temperature of 311 K. Figure 1.1 shows the upstream side of the cooler (flow traveling into the page).



Figure 1.1: K1 Cooler

The K1 Cooler consists of 72 individually controlled cooling bundles. The bundles are configured in a W configuration with six levels and twelve bundles on each level. See Figure 1.2 for a section view of the cooler. The bundles have two three-pass circuits that are stacked to create a six-layer bundle. Each bundle consists of 97 aluminum tubes. As seen below in Figure 1.3, air flows into the page through six levels of spiral finned tubes detailed in Figure 1.4. As seen in Figure 1.4, the headers and the 180-degree bends for each circuit are not in the airflow, but rather inside an inner and outer fairing. A typical piping configuration inside the fairings can be seen in Figure 1.5 and Figure 1.6. Due to the compact nature of the cooler bundles, it is not feasible to repair leaks since the only access to the tubes is from inside the fairings. For that reason, tubes are cut and the header is plugged to prevent water from releasing into the tunnel. It should be noted that Figure 1.5 and Figure 1.6 show tubes that have been cut and abandoned in place due to leaks.

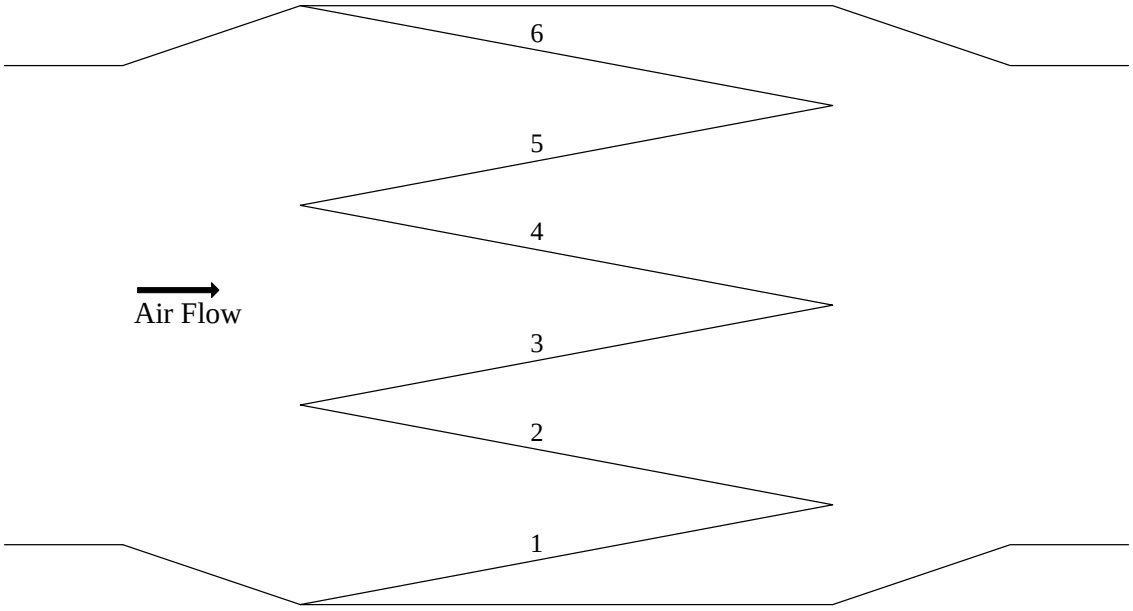


Figure 1.2: Section View of K1 Cooler



Figure 1.3: K1 Cooler Bundles

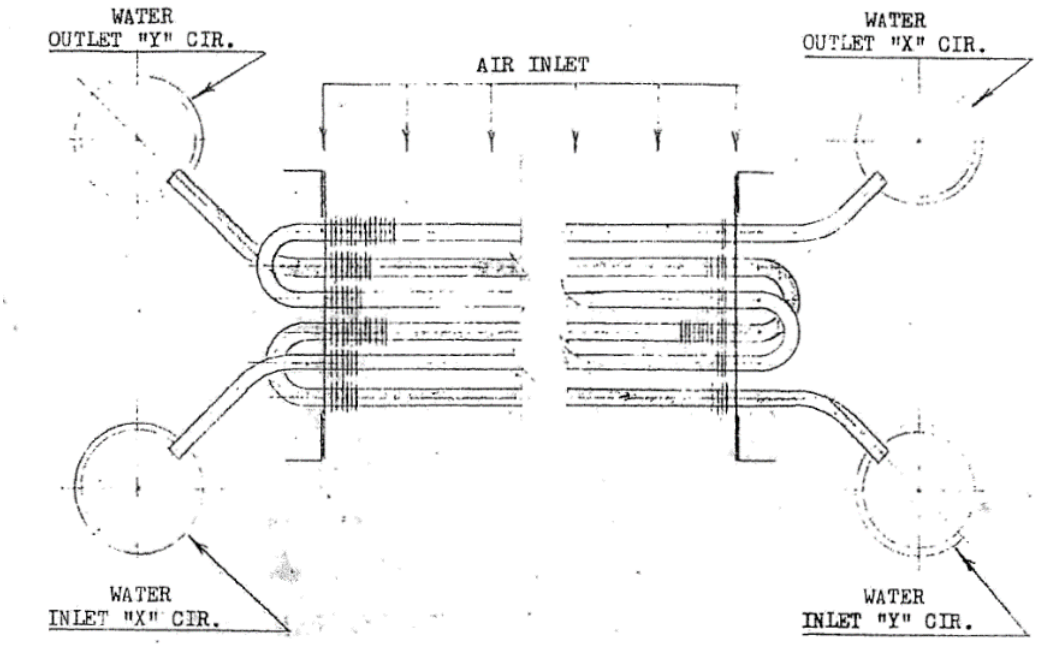


Figure 1.4: Section View of K1 Cooler Bundles

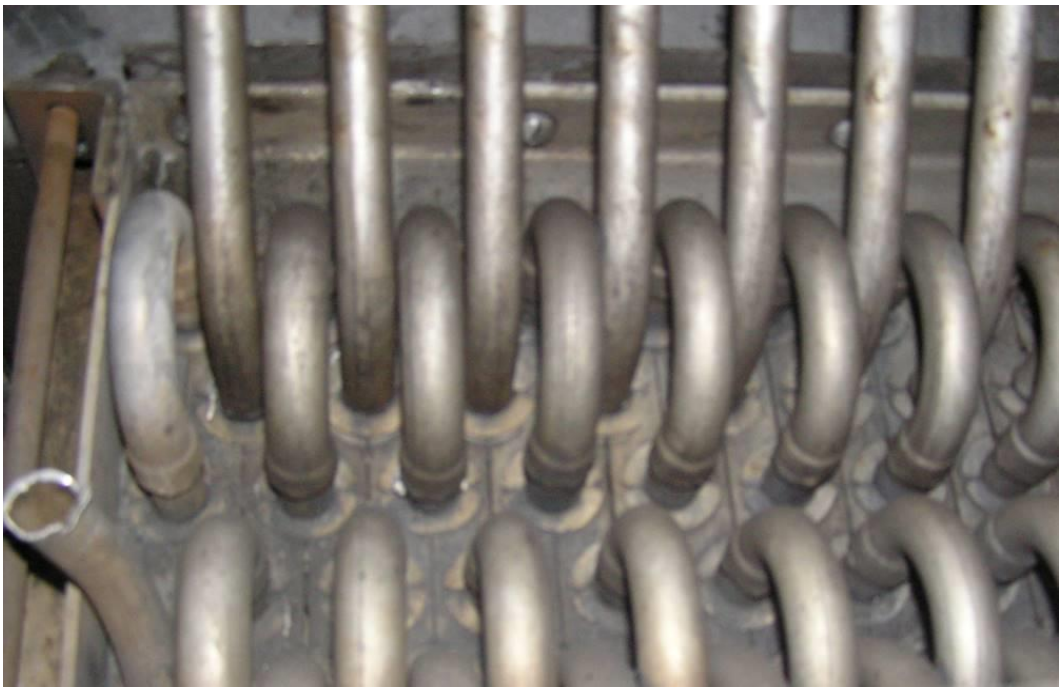


Figure 1.5: View of Bundle from Inside the Fairings



Figure 1.6: View of Bundle from Inside the Fairings

The K1 Cooler is supplied cooling water from the Woods Reservoir on Arnold AFB. While the reservoir is beneficial for providing large quantities of water (378,541 LPM for K1 Cooler), there are some problems with water quality. Although the water is filtered through a mesh screen before it is pumped into AEDC, fine particles (≤ 3 mm) and sediment are not removed. As a result, the K1 Cooler is still at risk for fouling due to sediment from the reservoir. To provide colder water to AEDC in the summer months, the distribution pump inlet duct is lowered to pull colder water from the bottom of the lake. As a result, the water becomes further contaminated from the sediment pulled in from the bottom of the reservoir. While the water may be colder, the added particles and sediment have proven to cause fouling in AEDC equipment.

Problem Statement

Throughout the years, the K1 cooler has struggled during the summer months to meet the 311 K test section temperature requirement. The cooler was originally designed for water at a temperature of 295 K. With elevated water temperatures up to 302 K, the cooler does not have the capacity to meet the 311 K test section temperature requirement. This problem received additional attention when 16T ceased operations because the K1 Cooler could not maintain test section temperature in the summer of 2015.

A project began in 2016 to determine in-situ performance of K1 and procure replacement bundles. This thesis seeks to investigate the impact of the effects of aging both from particulate fouling on the internal tube surface and loss of surface area due to leaking tubes. A tube was taken from a bundle installed in 2000 and dissected to identify the fouling layer composition and thickness profile. A Matlab code was created to predict cooler performance for varying fouling layer thicknesses and thermal conductivities. The core data was validated using empirical data collected during five 16T tests at various times of year. The question that this thesis seeks to answer is: how much additional capacity is required in the initial design of the cooler bundle to account for age related performance degradation?

CHAPTER TWO
LITERATURE REVIEW

Heat Exchanger Design

In theory, commercial air to water heat exchanger design can be simple. The inlet air and water temperatures are given. The exit air temperature is the design criteria and thus is given. In a system with a continuous water supply (river, reservoir, etc.) the exit temperature is not important because it does not have any effect on future supply temperature (as it does in a closed system). The thermal conductivity is known for common heat exchanger materials. Calculate the rate of heat transfer required for a given temperature difference and take in account size requirements, a heat exchanger can be purchased to meet the required temperature differential. However, further investigation is required to account for the issues that may occur in the future. Blindly increasing the capacity of the heat exchange may result in unnecessary cost increases, and underestimating the future degradation of capacity may result in an inability to meet requirements.

Fouling in Heat Exchangers

Fouling, to some degree, is an inevitable process that deteriorates the capability of heat transfer equipment. Mostafa M. Awad defines fouling as “the accumulation and formation of unwanted material on surfaces of processing equipment” [Awad, 2011]. According to multiple sources [Awad, 2011] [Kazi, 2012], fouling can adversely affect the operation of equipment in two ways. First, the fouling layer has a low thermal conductivity. This reduces the effectiveness of the heat exchanger since the layer is more resistant to heat transfer than the original heat transfer surface. Second, the cross sectional area is reduced as the fouling layer accumulates. This increases the pressure drop across the heat exchanger when maintaining the same flow rates.

Particulate Fouling

Particulate fouling is the accumulation of solid particles suspended in the system working fluid onto the heat surface. Heavy particles settle on the horizontal surfaces due to gravity; this is further classified as sedimentation fouling. The finer particles settle onto the heat transfer surface at different locations due to suction forces and other mechanisms [Kazi, 2012]. The main factors

that affect particulate or sedimentation fouling are fluid velocity (specifically regions of low velocity) and the concentration of suspended solids in the working fluid. While wall temperature has less of an effect of particulate/sedimentation fouling, a hot wall may cause the deposit to "bake on" and become difficult to remove [Ibrahim, 2012]. Typically, this type of fouling involves corrosion products dispersed in water, such as clay and mineral products from river water, soot particles from incomplete combustions, etc. [Awad, 2011].

Fouling Process

A fouling layer is created as a result of the net accumulation of fouling material caused by the simultaneous deposit and removal of material. The fouling factor (or fouling resistance, R_f) can be mathematically expressed as the difference between the deposition and removal rate, Φ_d and Φ_r respectively. All three parameters can be expressed in units of thermal resistance, $m^2 \cdot K/W$. See in Equation 2.1 and Figure 2.1.

$$R_f = \Phi_d - \Phi_r \tag{2.1}$$

Before fouling accumulation occurs on a clean/new heat exchanger, an initiation period or a time delay takes place. This delay is not predictable and appears to be random in nature [Awad, 2011]. Several authors reported negative fouling resistance (an increase in heat transfer capability) during the early stages of the fouling process. As illustrated in Figure 2.2. The initial accumulation can cause turbulence in the viscous layer, thus increasing the heat transfer coefficient at the interface between the fluid and the heat exchanger. This increase in heat transfer coefficient may overcome the thermal resistance of the deposits. This initial benefit continues until the added heat transfer resistance overcomes the advantage of the increased turbulence [Kazi, 2012]. For particulate fouling, the initiation period and roughness delay is very small.

Reza Razmavar further elaborates on the cause of the initiation period. He states that particles moving towards the surface may not necessarily stick to it. At the time of collision, the kinetic energy can be transferred from the particle to the surface. If the kinetic energy is greater than the adhesion force (between the particle and the surface), the particle rebounds. Likewise, if the adhesion force is greater, then the particle adheres to the surface [Razmavar, 2016].

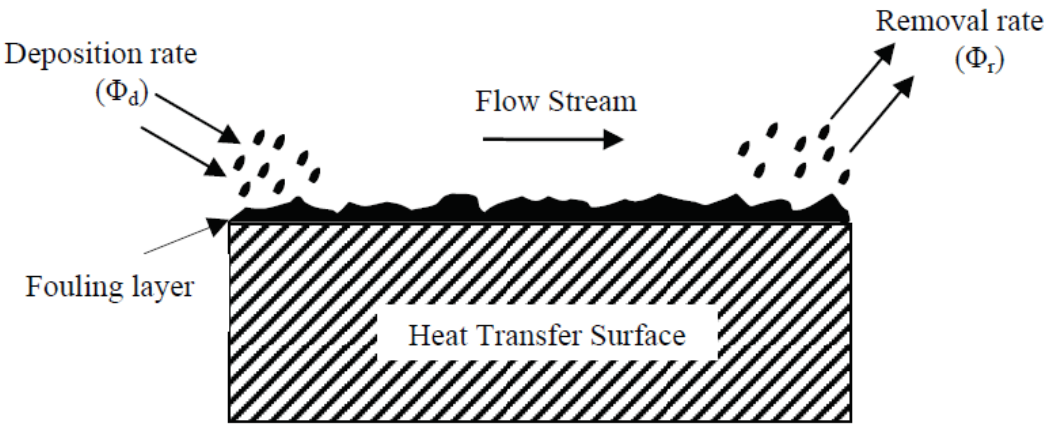


Figure 2.1: Typical Fouling Process [Awad, 2011]

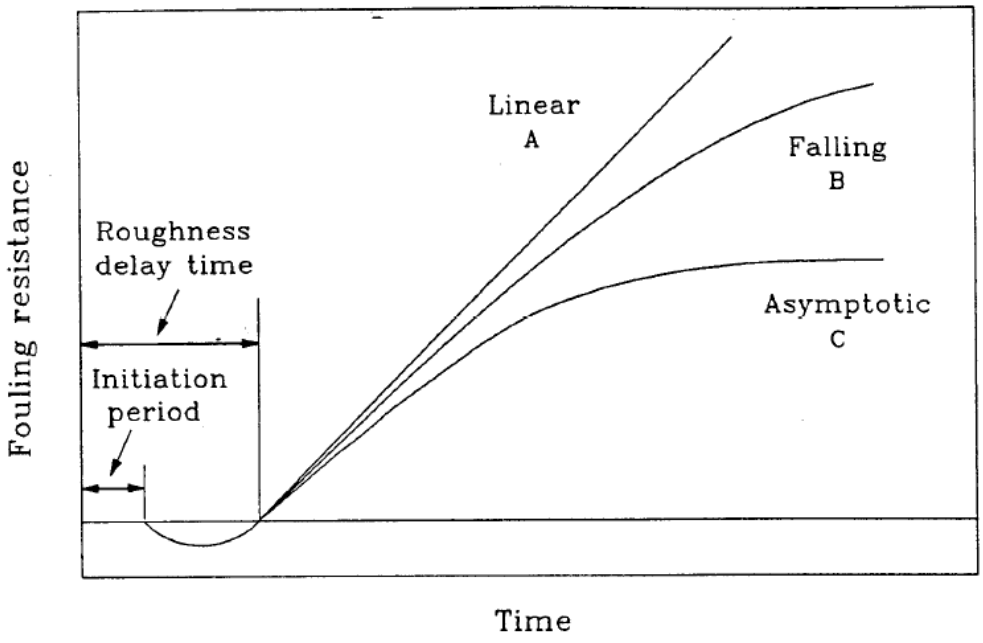


Figure 2.2: Typical Fouling Curves [Kazi, 2012]

After the initiation and roughness delay, the fouling curve can be classified by three ideal curves: Linear, Falling, and Asymptotic. For particulate fouling, fouling resistance typically increases along an asymptotic curve. As the fouling layer increases in thickness, the cross-sectional area decreases, thus causing an increase in the fluid velocity and increasing the shear stress. The increased shear forces are greater than the bonding forces between the particles and the wall. At the asymptote, the removal rate is equal to the deposit rate. [Awad, 2011] [Kazi, 2012].

The balance of forces between the fluid, particle, and surface determine whether the fouling particles will adhere to the surface and accumulate or disperse with the fluid. Figure 2.3 provides a schematic of the forces acting on the attached particle in a fluid flow. The fluid is flowing from left to right at a given velocity resulting in a drag force, F_D, on the particle. The drag force is a function of fluid velocity and particle size. The greater the fluid velocity or particle diameter, the greater the drag force. The Van der Waal adhesion force between the particle and the surface (or other particles in the case of an accumulating fouling layer) is shown by F_V. As shown in Figure 2.3, the attraction force is normal to the contact diameter. The lift and weight forces are given by F_L and F_W, respectively [Razmavar, 2016]. The direction of the weight force is dependent on the orientation of the surface in contact with the fouling particle. Given that gravity is only applied in one direction, the weight force may be pulling away from the surface.

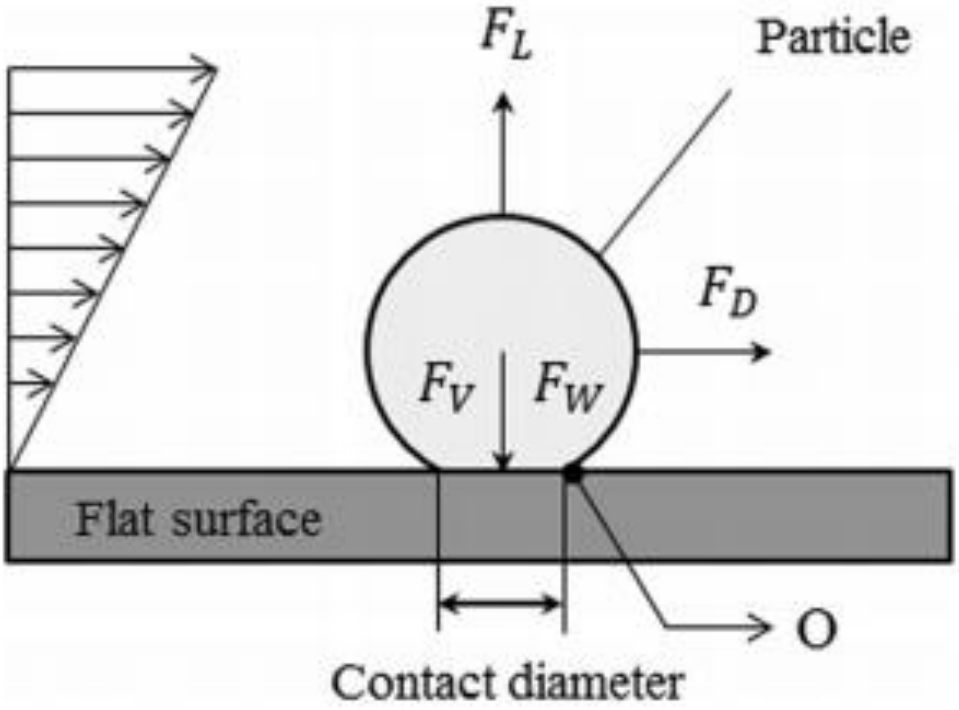


Figure 2.3: Forces Acting on Fouling Particle [Razmavar, 2016]

Quantifying Fouling Accumulation

Fouling layer thickness follows a similar curve to the asymptotic fouling resistance curve, shown in Figure 2.4 [Kazi, 2012]. After an initial accumulation period, the thickness increases at a linear rate until the growth levels out at the maximum thickness. As described above, this is attributed to the increased velocity caused by a reduced cross-sectional flow area.

Multiple techniques exist to quantify the accumulation of fouling in heat exchangers. The method used is determined based on the specifics of the heat exchanger itself.

The simplest method is directly weighing the heat exchanger. If the installed weight is known, the mass of the accumulated fouling can be determined by simply subtracting the "clean" weight from the fouled weight [Awad]. This process becomes more difficult with larger heat exchangers that are not easily removed. The larger the heat exchanger, the more expensive and labor intensive it is to remove and reinstall. In addition, larger scales tend to be less sensitive to small changes that may be caused by the increase in mass from the fouling layer.

The second method is fouling layer thickness measurements. This method requires access to the internal surface of the heat exchanger (or the tubes of a tubed heat exchanger). If initial measurements are taken before installation, the fouling layer thickness can be determined by the increased thickness of the fouled tube. If initial measurements are not taken, the thickness of the fouled surface can be measured and again with the fouling layer removed. The fouling layer thickness can be calculated as the difference between the thickness of the fouled surface and the thickness of the "clean" surface. The thickness measurements completed for this analysis are described in further detail in the following section.

The third method is heat transfer measurements. This is the least intrusive method and may be the only option if access to the heat exchanger is not feasible. Fouling resistance can be calculated as a difference between the overall heat transfer coefficient of a fouled heat exchanger and a clean heat exchanger [Awad]. See Equation 2.2.

$$R_f = \frac{1}{U_f} - \frac{1}{U_c} \tag{2.2}$$

This study required additional heat transfer analysis to validate the fouling resistance and further define the effect of the fouling layer on overall heat exchanger performance. This is due to the

unknown composition of the fouling layer. As detailed in the following sections, the thermal conductivity was estimated by comparing calculated results for varying values of thermal conductivity to empirical data. This was used to calculate the change in air temperature, change in water temperature, and overall heat transfer based on fouling layer thickness.

Another method is measuring the pressure drop between the inlet and exit of the internal fluid. This is typically done in conjunction with other methods. As the cross-sectional area decreases due to an increasing fouling layer thickness, the resulting downstream pressure will decrease with the increasing flow velocity [Awad, 2011]. This becomes more difficult when multiple inlets or exits are combined in a common manifold or the manifolds are difficult to instrument as was found in this specific study. Other methods such as radioactive traces, laser techniques, and infrared systems can also be used to assess the accumulation of a fouling layer.

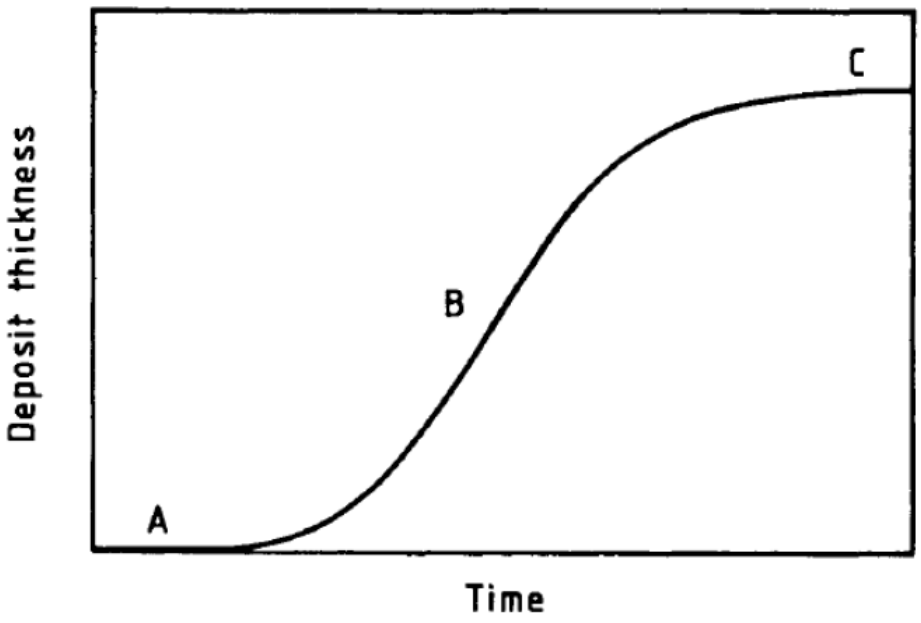


Figure 2.4: Typical Fouling Layer Accumulation Curve [Kazi, 2012]

Fouling Resistance Calculations

Multiple models have been created to provide a mathematical model to predict the fouling resistance (R_f) for a given fouling layer. One of the earliest models of fouling is that by Kern and Seaton [Awad, 2011]. In this model, it is assumed the rate of deposition mass, $\dot{m}_d$, remains constant with time, but the rate of removal mass, $\dot{m}_r$, is proportional to the accumulated mass, $\dot{m}_f$, and increases with time to approach the deposition mass asymptotically. Given that the rate of accumulation is equal to the rate of deposition minus the rate of removal, Equation 2.3 can be integrated from the initial conditions $\dot{m}_f = 0$ and $t = 0$ to give Equation 2.4.

$$dm_f/_{dt} = \dot{m}_f = \dot{m}_d - \dot{m}_r \tag{2.3}$$

$$m_f = m_f^*(1 - e^{-\beta t}) \tag{2.4}$$

Where m_f^* is the asymptotic value of m_f and $\beta = 1/t_c$, with t_c representing the average residence time for an element of fouling material at the heat transfer surface. The accumulated mass per unit area, m_f, of the fouling layer can be further quantified as a function of fouling resistance, R_f, the density of the foulant, ρ_f, the thermal conductivity, k_f, and the thickness of the fouling layer (x_f) by Equation 2.5.

$$m_f = \rho_f x_f = \rho_f k_f R_f \tag{2.5}$$

The fouling resistance is further defined by the fouling layer thickness divided by the thermal conductivity of the foulant as in Equation 2.6.

$$R_f = \frac{x_f}{k_f} \tag{2.6}$$

Referencing Equations 2.4 and 2.5, the fouling resistance can be expressed as a function of time and the asymptotic fouling resistance, R_f^*.

$$R_f = R_f^*(1 - e^{-\beta t}) \tag{2.7}$$

It has been noted that Equation 2.7 does not provide a quantitative value for fouling resistance, but an expression for the asymptotic fouling resistance as a function of variables that affect the fouling process.

J.G. Knudsen analyzed fouling resistance as the result of a degrading overall heat transfer coefficient, Equation 2.2. Solving for the overall heat transfer coefficient of the fouled surfaces results in Equation 2.8.

$$U_f = \frac{U_c}{1 + U_c R_f} \tag{2.8}$$

Substituting Equation 2.7 into Equation 2.8:

$$U_f = \frac{1}{\frac{1}{U_c} + R_f^*(1 - e^{-\beta t})} \tag{2.9}$$

If the values of the two coefficients R_f^* and t_c can be obtained either empirically or analytically, then Equation 2.9 can be used as a method for predicting fouling factor in the heat exchanger design [Awad, 2011].

CHAPTER THREE
MATERIALS AND METHODS

Instrumentation of K1 Cooler

In order to accurately determine the thermal characteristics of the fouling layer, experimental data was required for the supply and discharge temperatures on both the airside and waterside of the heat exchanger. The existing cooler infrastructure provided water side supply temperature and air side discharge temperature. The water supply temperature is taken at the inlet isolation valves located approximately twenty meters upstream of the bundles. It is assumed that any change in temperature from the isolation valves to the bundle header is negligible. The airside discharge temperature is measured by resistance temperature detectors (RTDs) mounted directly to the discharge side of the bundle. See Figure 3.1 below.

As described in Chapter 1, the K1 Cooler is configured inside a circular duct. As a result, bundle lengths vary depending on which level the bundle is located on. The shorter bundles (Level 1 and 6) have one RTD per bundle and the larger bundles (Level 2-5) have two. For the larger bundles, the discharge valve position is based on an average between the two temperature readings. See Figure 3.2 for typical RTD locations.

Six RTDs were installed on the K1 center fairing to measure the inlet air temperature. See Figure 3.3. RTDs were mounted to the north and south side of the fairing on each level. The values from the six RTDs were averaged to provide an inlet temperature to the K1 Cooler.

The individual bundle water headers are enclosed in the center and outer fairings. It was not practical to install RTDs on multiple bundles for this study. For that reason, an average was measured. All seventy-two bundles drain into a single sump pit before draining out the 72-inch return line. Figure 3.4 shows water draining into the sump pit. The water side discharge temperature was measured in this vault. Each bundle discharge valve modulates to create a uniform temperature distribution across the cooler. For this reason, the difference in discharge water temperature is assumed to be uniform from bundle to bundle. A RTD was submerged into the pit to measure the bundle discharge temperature.



Figure 3.1: Downstream RTDs

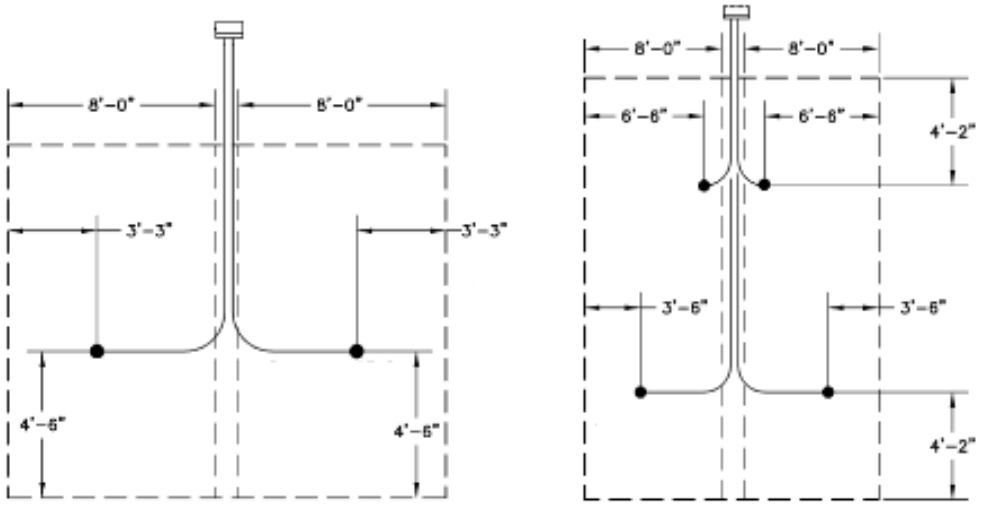


Figure 3.2: Typical RTD location for Levels 1 and 6 (left) and Levels 2-5 (right)



Figure 3.3: Upstream RTDs – Air Side



Figure 3.4: K1 Cooler Sump Pit – Location of Discharge RTD

Fouling Layer Investigation

Fouling Layer Thickness Measurements

As it was previously noted, it was observed that the cooler tubes were lined with a layer of sediment. The thickness and composition of this layer was unknown due to access to the inside of the tube. To further investigate, a tube was removed from the cooler. The tube was installed in 2000 and was active until its removal in 2017. The tube was cut down the length of the tube to allow access to the inside surface of the tube. The internal surface of tube can be seen in Figure 3.5. The fouling layer was smooth to the touch and required heavy scraping to be removed.

The tube was inspected using a microscope to further investigate the surface condition of the fouling layer. Under the microscope (Figure 3.6), it became apparent that the layer was porous and potentially not as consistent as it was first concluded.

Investigation to the fouling layer with an electron scanning microscope by a field emission SEM JEOL JSM-6320F further confirmed the porosity and inconsistency in the fouling layer. Figure 3.7 is a plan view and Figures 3.8 and 3.9 are section views of the fouling layer. The cross section of the Aluminum tube can be seen at the bottom of Figures 3.8 and 3.9 with the fouling layer sitting flush on the face.



Figure 3.5: Internal Surface of Tube



Figure 3.6: Magnified View of Tube Surface

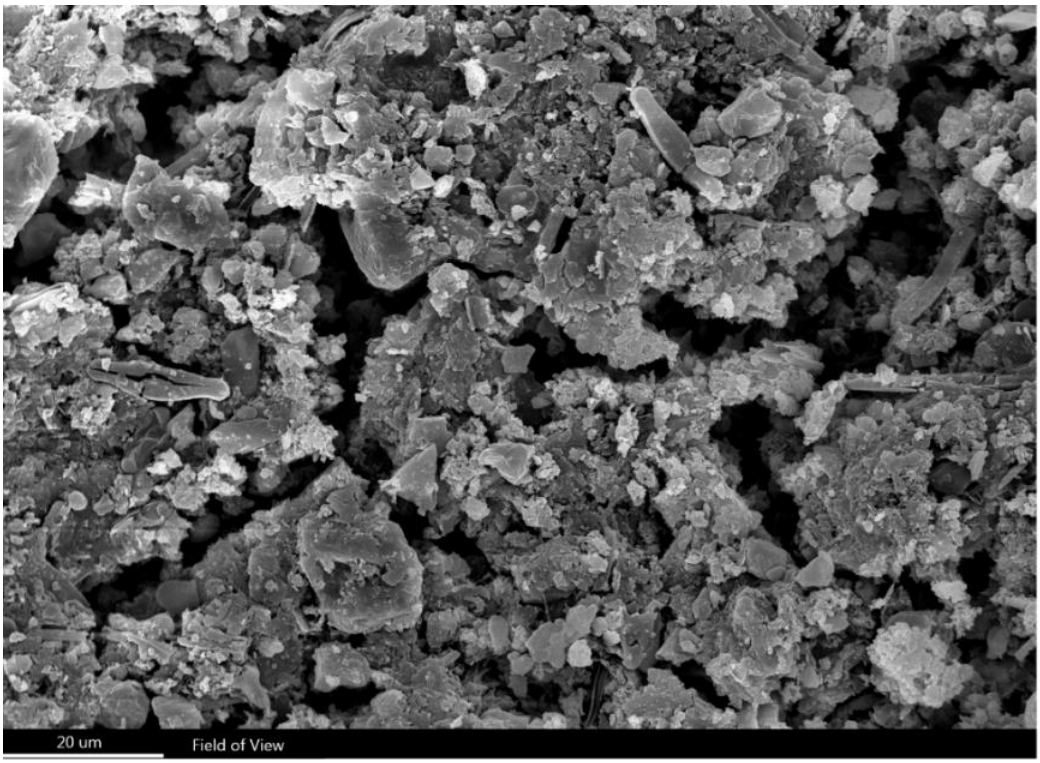


Figure 3.7: Plan view of Fouling Layer

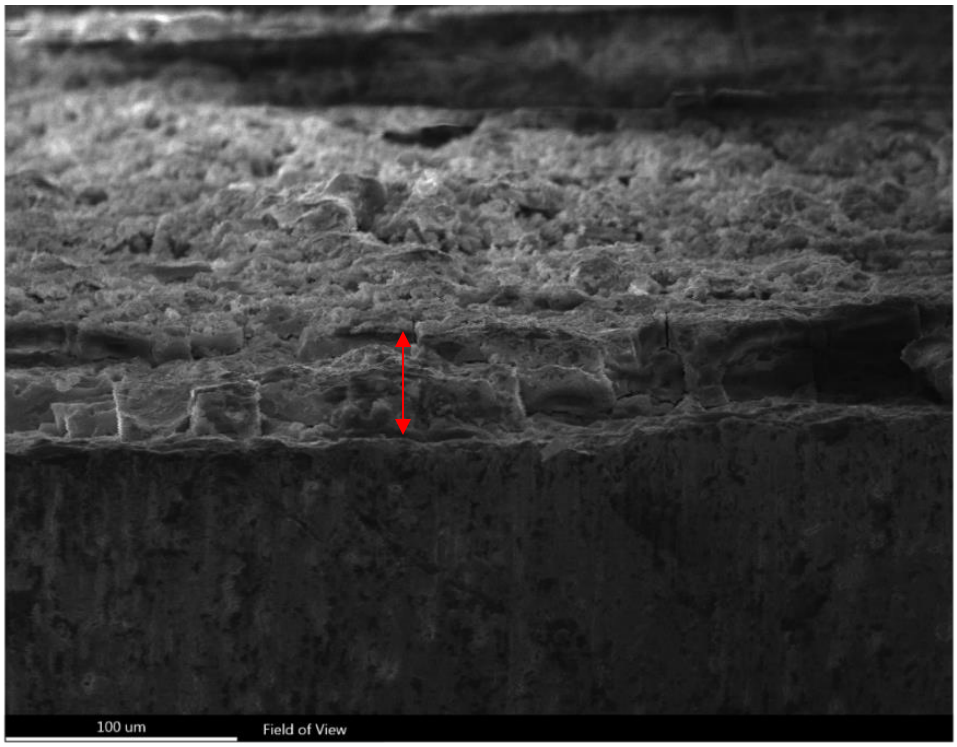


Figure 3.8: Section View

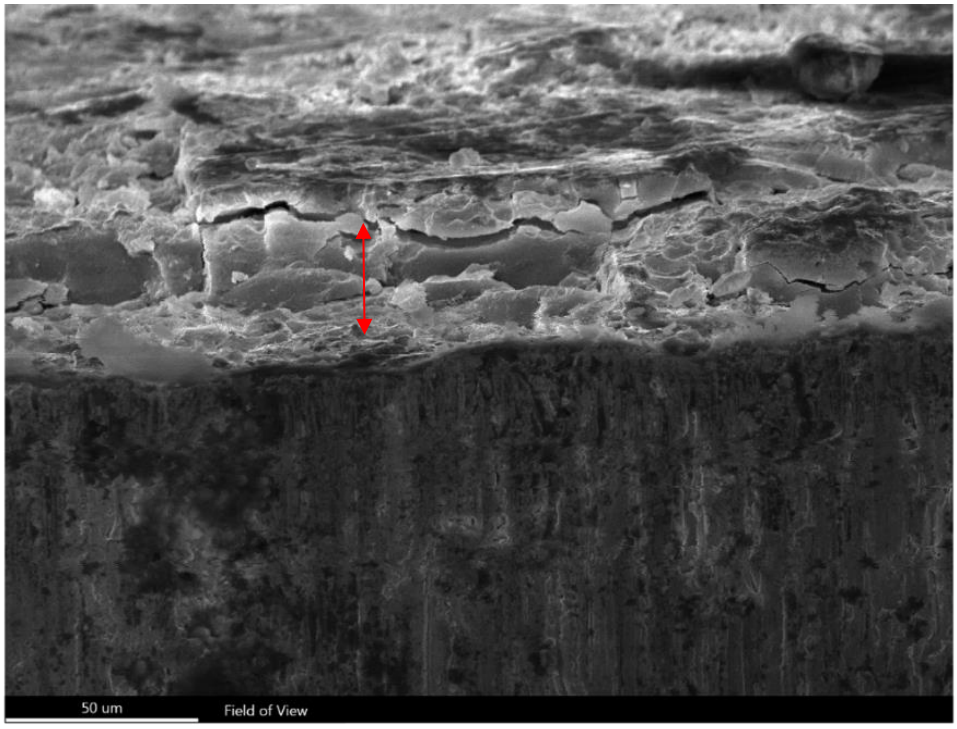


Figure 3.9: Zoom-in Section View

The thickness of the fouling layer was measured by using a before and after method. The thickness of the tube was measured then the layer was removed and the tube thickness was measured again. Unfortunately, the fouling is not uniform across the entire inner surface. To find the most accurate value, seven measurements were taken on the sample tube and an averaged value was used in this analysis. Table 3.1 shows the thickness measurements found on the tube.

Table 3.1: Sample Tube Thickness

	With Fouling [mm]	Without Fouling [mm]	Fouling Layer Thickness [μm]
#1	1.803	1.702	101
#2	1.854	1.651	203
#3	1.778	1.676	102
#4	1.803	1.651	152
#5	1.829	1.651	178
#6	1.778	1.651	127
#7	1.829	1.702	127
Average Fouling Layer Thickness			**141**

Fouling Layer Composition

The composition of the fouling layer was determined by energy dispersive spectrometry (EDS) using an EDAX Octane plus Silicon Drift Detector with EDAX's TEAM EDS in the electron scanning microscope of a field emission SEM JEOL JSM-6320F. Table 3.2 shows the composition found in the tube sample.

As expected, the fouling layer consists of typical earth elements that would be commonly found in dirt and lake water. As stated previously, the cooling water for AEDC is provided from Woods Reservoir. High flow rate requirements prevent the possibility of filtering tiny particles and sediment pulled from the bottom of the lake. These particles end up in the test facilities and result in particulate fouling.

The increase in iron is expected to be caused by the aging of the carbon steel distribution piping. As pipes age, it is more likely that rust (or iron oxide) particles from the inner diameter of the pipe mix with the water.

Table 3.2: Fouling Layer Composition (%)

	Mg	**Si**	**P**	**S**	**Ca**	**Mn**	**Fe**	**Cu**	**Total**
Sample 1	7.40	20.93	4.79	1.14	12.90	14.38	35.18	3.28	100
Sample 2	7.85	21.76	6.44	0.99	13.75	11.93	34.09	3.19	100
Sample 3	8.38	22.94	6.47	1.32	13.70	12.65	31.75	2.79	100

Cooler Bundle Analysis

Model of Cooler Bundle

Due to multiple investment projects to replace degraded cooler bundles, the K1 cooler consists of multiple iterations of bundles. All bundles consist of aluminum tubes and aluminum fins that are dimensionally the same. This particular study will focus on the most recent bundles that were installed in 2000. The bundles have a spiral wrapped fin that is not attached, but rather rests (See Figure 3.10) on the outside diameter of the tube. The fins have a smooth mill run finish without any additional corrugations.

For this analysis, a simplified model was used. The tubes have an outer diameter of 22.2 mm and a thickness of 1.65 mm (or an inner diameter of 18.9 mm). The fins are circular with a diameter of 47.6 mm and a thickness of 0.30 mm. Rather than a continuous helix that spans the length of the bundle, the fins were modeled as straight fins (fully attached to the tube) that are spaced 3.28 mm face to face as shown in Figure 3.12 and Figure 3.13. See section view in Figure 3.11. Figures 3.14 and 3.15 were created to better illustrate the fouling layer thickness compared to the tube thickness.

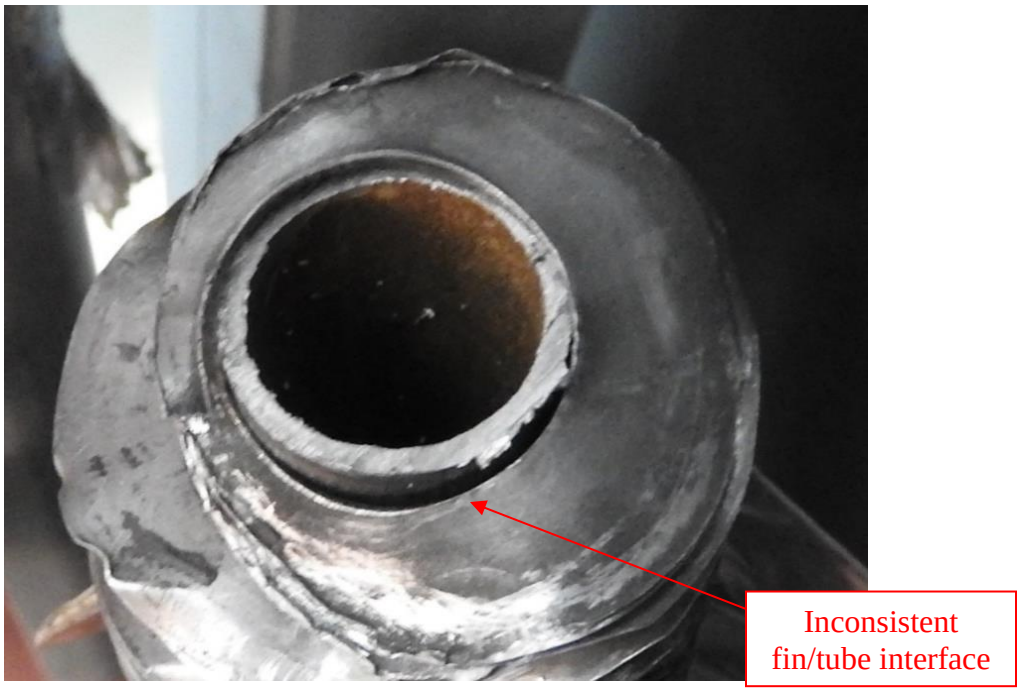


Figure 3.10: K1 Cooler Tube

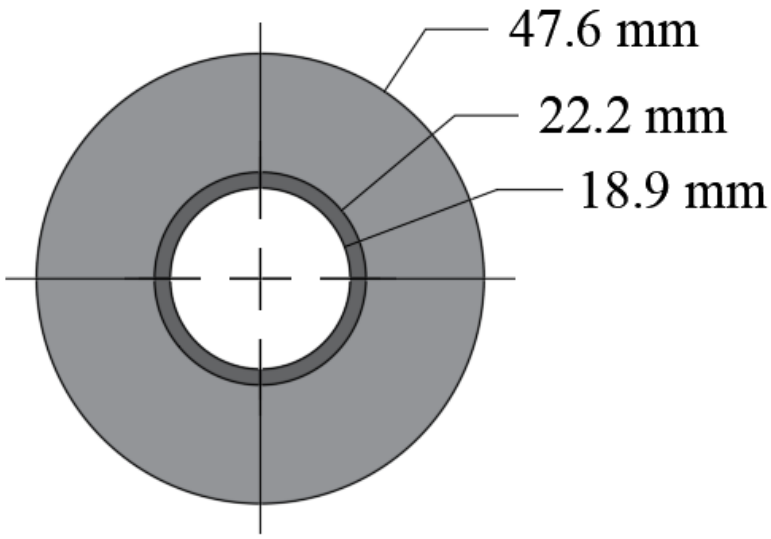


Figure 3.11: Typical Cross Section View of Tube

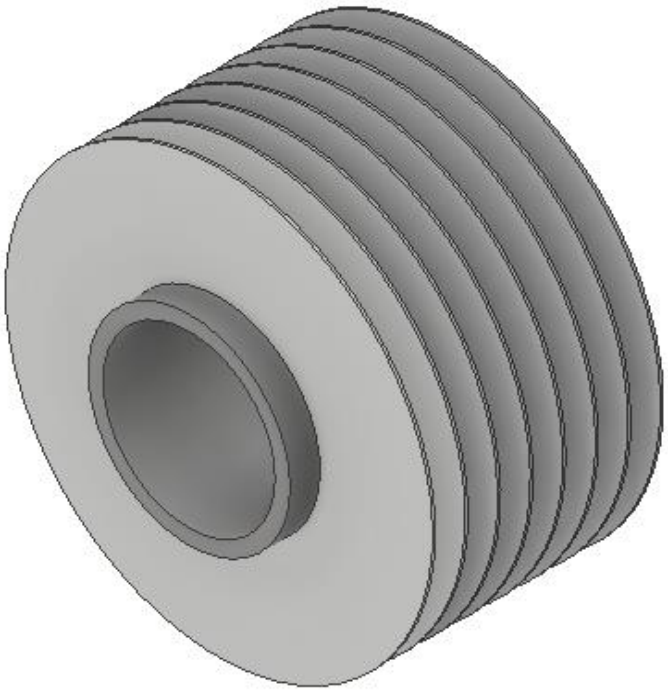


Figure 3.12: Typical Cooler Bundle Tube

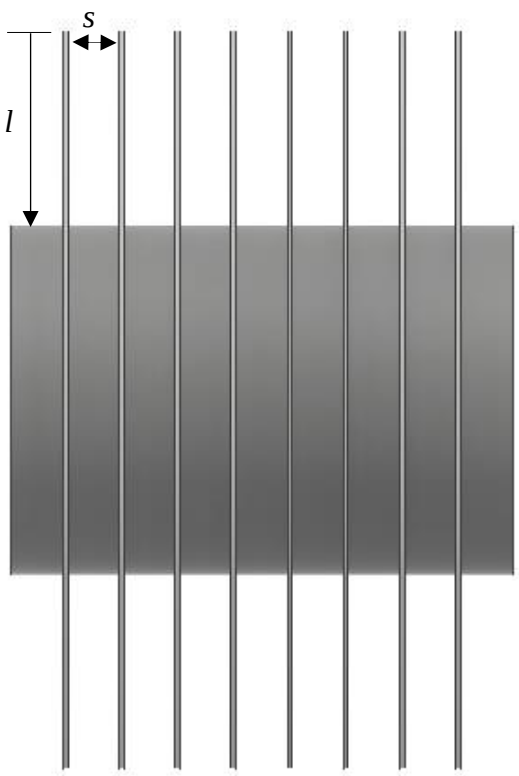


Figure 3.13: Side View of Cooler Bundle Tube

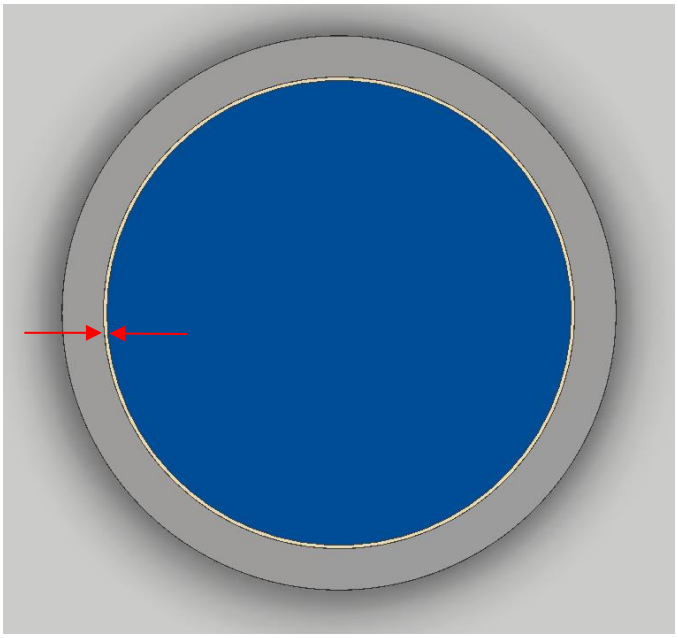


Figure 3.14: 141 µm Fouling Layer

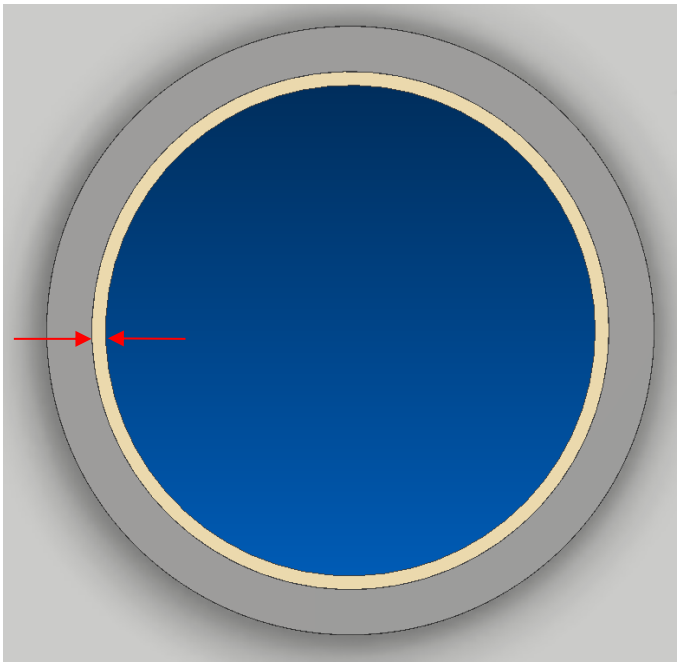


Figure 3.15: 500 µm Fouling Layer

General Assumptions

- Bundles are composed of a simplified tube/fin combination described previously in this chapter.
- Fin and tube are assumed to be a continuous conductive layer.
- The average fouling layer thickness found is assumed to be representative of the entire bundle.
- K1 inlet air is fully mixed, and T_{t4} is the same for all bundles.
- For all bundles, K1 inlet and exit water temperatures are the same.
- Thermal loss is neglected around the tunnel ($T_{t1} = T_{t2}$ & $T_{t3} = T_{t4}$).
- Changes in ducting diameter act as isentropic nozzles.
- Mass is conserved around the tunnel and density is assumed to be constant for subsonic flow.
- Inlet air and water distribution is assumed to be equally distributed between all seventy-two bundles.
- The bundle inlet air velocity is assumed to be equal to the velocity at inlet to the cooler.

16T Airside Parameter Locations

As previously discussed, the installation of instrumentation was required around the K1 Cooler to provide critical parameters (for instance: inlet air temperature, exit water temperature, etc.). Any additional parameters had to be calculated from other areas in the tunnel where the data was available. For simplification, the airside areas were labeled from one to five starting at the 16T test section, as seen in Figure 3.16. This paper will use the following nomenclature when assigning subscripts to common airside parameters:

1 – Test Section

2 – Compressor Inlet

3 – Compressor Exit

4 – K1 Cooler Inlet

5 – K1 Cooler Exit

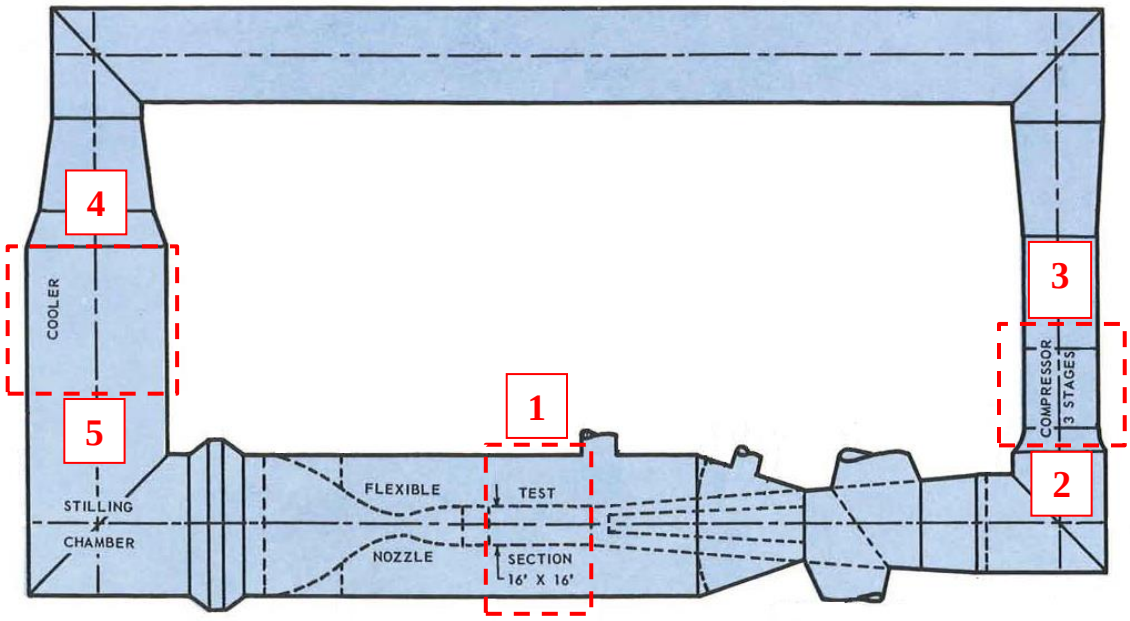


Figure 3.16: Illustration of 16T Airside Parameter Location

Convection Heat Transfer Analysis

The first step in the analysis was calculating the area for the tube. As described in Chapter 1, the cooler bundles consist of two three-pass circuits. The two 180-degree bends in each circuit are not the air flow, but rather inside the inner and outer fairings, reference Figure 3.15 above. For this reason, the length of the tube was calculated as a product of the airside length and the number of passes for each circuit, as shown in Equation 3.1.

$$A_{tube} = \pi d_o L_{tube} N_{pass} \tag{3.1}$$

The total area of each tube includes both the outside surface area of the tube and the surface area of each fin (Equation 3.2). The overall airside surface area of the bundle (Equation 3.3) is the sum of the tube and fin surface areas multiplied by the total number of tubes in the bundle.

$$A_{fin} = N_{fin}\left[\frac{\pi}{2}\left(d_{fin}^2 - d_o^2\right) + \pi \cdot d_{fin} \cdot x_{fin}\right] \tag{3.2}$$

$$A_{tube_total} = N_{tube}\left(A_{tube} + A_{fin}\right) \tag{3.3}$$

As described above, some of the parameters required for this analysis had to be calculated from areas other than K1 to allow for a more accurate comparison to the experimental data. The mass flow was calculated for each test based on measuring conditions in the test cell. Isentropic relations (Equations 3.4 and 3.5) were used to find the static conditions and ultimately the density and mass flow [Anderson, 2004].

$$T_1 = T_{t1}\left(1 + \frac{\gamma - 1}{2} {M_1}^2\right)^{-1} \tag{3.4}$$

$$P_1 = P_{t1}\left(1 + \frac{\gamma-1}{2} {M_1}^2\right)^{\frac{-\gamma}{\gamma-1}} \quad \text{or} \quad P_1 = P_{t1}\left(\frac{T_1}{T_{t1}}\right)^{\frac{\gamma}{\gamma-1}} \tag{3.5}$$

For Equations 3.4 and 3.5, the specific heat ratio of air ($\gamma = 1.4$) is assumed constant for all test conditions. To calculate density (ρ), Equation 3.6 utilizes the Ideal Gas Law.

$$\rho_1 = \frac{P_1}{RT_1} \quad where \quad R = 286\ {}^{J}/_{kg \cdot K} \tag{3.6}$$

The mass flow rate in the test cell was calculated from Equation 3.8 and the velocity is defined as the Mach number multiplied by the speed of sound (Equation 3.7).

$$V_1 = M_1\sqrt{\gamma RT_1} \tag{3.7}$$

$$\dot{m}_1 = \rho_1 V_1 A_1 \tag{3.8}$$

From the Law of Conservation of Mass, the mass flow is assumed be constant from the test cell to the inlet to the K1 cooler. See Equation 3.9. For simplification, density is also assumed to be constant around the tunnel for subsonic flow, per Equation 3.10.

$$\dot{m}_4 = \dot{m}_1 \tag{3.9}$$

$$\rho_4 = \rho_1 \tag{3.10}$$

For supersonic test conditions, the density is calculated again using the isentropic relationships downstream of the diffuser (location #2 on Figure 3.16) once the flow velocity is decreased to subsonic before it enters the compressor. Utilizing the isentropic flow tables [Anderson, 2004], the Mach number between the diffuser and the compressor inlet (M_2) was calculated based on the compressible area ratio, Equation 3.11 below. Where A_1/A^* is found based on the known test cell Mach number (M_1).

$$\frac{A_2}{A^*} = \frac{A_2}{A_1}\frac{A_1}{A^*} \tag{3.11}$$

Once A_2/A^* is calculated, M_2 can be looked up in the isentropic tables. T_2, P_2, and ρ_2 can be calculated by repeating Equations 3.4 – 3.6 for location #2. For supersonic test conditions Equation 3.10 is replaced by Equation 3.12.

$$\rho 4 = \rho 2 \tag{3.12}$$

Since the area of the K1 duct is known, the velocity of the air entering the K1 cooler is calculated by Equation 3.13.

$$V_4 = \frac{\dot{m}_4}{\rho_4 A_4} \tag{3.13}$$

Substituting Equation 3.14 from the First Law of Thermodynamics into the general equation for total enthalpy (Equation 3.15), Equation 3.16 was used to find the static temperature at the inlet to the K1 Cooler (T_4) [Bejan, 2013].

$$h = c_p T \text{ and } h_t = c_p T_t \tag{3.14}$$

$$h_t = h + \frac{V^2}{2} \tag{3.15}$$

$$T_4 = T_{t4} - \left(\frac{{V_4}^2}{2c_{p,air}}\right) \tag{3.16}$$

As shown in Equation 3.17, Sutherland's Formula [Bejan, 2013] was utilized to find viscosity entering K1.

$$\mu_4 = \mu_o \left(\frac{T_o + C}{T + C}\right)\left(\frac{T}{T_o}\right)^{\frac{3}{2}} \tag{3.17}$$

$$For\ air: \quad C = 120K, To = 291.15K, \mu_o = 18.27\mu Pa \cdot s$$

With the viscosity of air calculated in Equation 3.17, the Reynold's number can be calculated based on the tube outside diameter as the characteristic length, Equation 3.18.

$$Re_a = \frac{D_{o,tube} V_4 \rho_4}{\mu_4} \tag{3.18}$$

The Prandtl number was calculated per Equation 3.19.

$$Pr_a = \frac{\mu_a c_{p,a}}{k_a} \tag{3.19}$$

Piotr Wais's *Fin-Tube Heat Exchanger Optimization* study was utilized to find the average Nusselt number by Equation 3.20 [Wais, 2012]. Equation 3.20 is only applicable for staggered tube banks and is bounded by the following parameters:

$2x10^3 \leq Re \leq 4x10^4$, $0.13 < \frac{s}{l} < 0.57$, $1.15 < \frac{X_T}{X_L} < 1.72$

$$\overline{Nu}_a = 0.242 Re_{air}^{0.658} \left(\frac{s}{l}\right)^{0.297} \left(\frac{X_T}{X_L}\right)^{-0.091} Pr_{air}^{0.33} \tag{3.20}$$

The lateral and transverse distances (X_L and X_T) for a staggered cross-flow heat exchanger are defined in Figure 3.17. Wais also included a multiplier in the Nusselt Number calculation (Equation 3.20) for fluid property variation at high temperatures and for bundles with less than four rows. However, neither are applicable for this particular study, so both were removed from the referenced equation resulting in a simplified Equation 3.20.

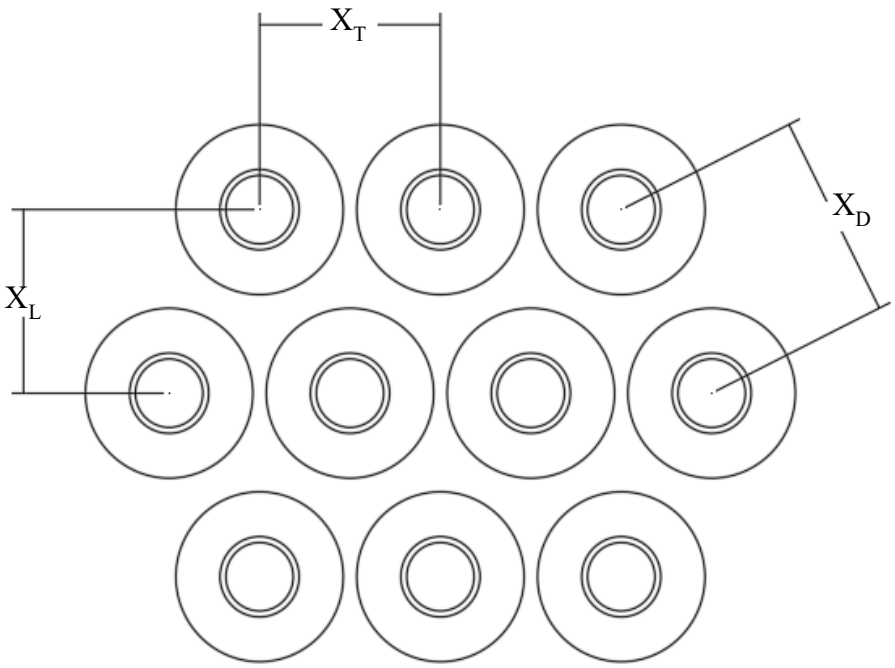


Figure 3.17: Schematic of Bundle Arrangement

The result from Equation 3.20 is substituted into Equation 3.21 to find the convective heat transfer coefficient for the airside.

$$h_a = \frac{\overline{Nu_a} \cdot k_a}{D_{o,tube}} \tag{3.21}$$

The waterside analysis allows for a much simpler approach since the required parameters are more readily available. The water velocity is calculated based on the distribution of a known mass flow coming into the cooler. The cooler supply piping that is used to supply all seventy-two bundles decrease in diameter with increases in elevation. For this reason, it is assumed that the water flow is distributed between each bundle equally and pressure losses due to elevation are negligible. Based on these assumptions, Equation 3.22 can be used to find the water velocity entering the tube.

$$V_w = \frac{\dot{m}_w}{N_{tube} \cdot N_{bundle} \cdot \rho_w \cdot A_{i,cs}} \tag{3.22}$$

Where the tube internal cross section is defined by Equation 3.23.

$$A_{i,cs} = \frac{\pi(d_{i,tube} - 2\delta_{foul})^2}{4} \tag{3.23}$$

Total Internal surface area was defined by Equation 3.24.

$$A_i = \pi d_{foul} L_{tube,total} \tag{3.24}$$

Where the overall tube length for the entire bundle and inner diameter of the fouling layer are defined by Equations 3.25 and 3.26.

$$L_{tube,total} = L_{tube} N_{pass} N_{tube} \tag{3.25}$$

$$d_{foul} = d_i - 2\delta_{foul} \tag{3.26}$$

Reynolds number was calculated by the standard formula for flow inside a pipe (Equation 3.27).

$$Re_w = \frac{d_{foul} V_w \rho_w}{\mu_w} \tag{3.27}$$

Similar to the air side analysis, the formula for Prandtl number is given by Equation 3.28.

$$Pr_w = \frac{\mu_w c_{p,w}}{k_w} \tag{3.28}$$

The Dittus-Boelter Equation for turbulent flow inside a pipe is shown by Equation 3.29 [Bejan, 2013].

$$Nu_w = (0.0243) {Re_w}^{0.8} {Pr_w}^{0.4} \tag{3.29}$$

The formula for the Nusselt number is rearranged into Equation 3.30 and the equation is solved for the convective heat transfer coefficient for water.

$$h_w = \frac{Nu_w k_w}{d_{i,tube} - 2\delta_{foul}} \tag{3.30}$$

The overall heat transfer coefficient is defined by 3.31. In this particular study, the fouling layer is treated as a second wall resistance (as seen in the last term of Equation 3.31) [Lee, 2013].

$$\frac{1}{UA} = \frac{1}{h_w A_i} + \frac{1}{h_a A_o} + \frac{\ln\left(\frac{d_o}{d_i}\right)}{2\pi k_{AL} L_{tube,total}} + \frac{\ln\left(\frac{d_i}{d_{foul}}\right)}{2\pi k_{foul} L_{tube,total}} \tag{3.31}$$

The heat transfer across the bundle is found by Equation 3.33 where the log mean temperature difference is shown in Equation 3.32 [Lee, 2013].

$$\Delta T_{LM} = \frac{(T_4 - T_{wi}) - (T_5 - T_{wo})}{\ln \frac{(T_4 - T_{wi})}{(T_5 - T_{wo})}} \tag{3.32}$$

$$Q_{bundle} = UA\Delta T_{LM} \tag{3.33}$$

The convective heat transfer for the air and water was found as a function of mass flow and temperature difference in Equation 3.34 and 3.35 [Bejan, 2013].

$$Q_{air} = \left(\frac{1}{N_{bundle}}\right)\dot{m}_a c_{p,a}(T_4 - T_5) \tag{3.34}$$

$$Q_{water} = \left(\frac{1}{N_{bundle}}\right)\dot{m}_w c_{p,w}(T_{wo} - T_{wi}) \tag{3.35}$$

Taking advantage of the energy balance across the cooler bundle, Equations 3.33 – 3.35 were substituted into Equation 3.36 and solved simultaneously as a system of equations to find the two unknowns: T_5 and T_{wo}.

$$Q_{bundle} = Q_{water} = Q_{air} \tag{3.36}$$

CHAPTER FOUR
RESULTS AND DISCUSSION

Fouling Layer Thermal Conductivity Analysis

As previously stated, the "as new" performance of the K1 Cooler is not known. As a result, the value of thermal conductivity for the fouling layer is a bit more complicated to predict. An initial assumption was that the fouling layer would have a thermal conductivity comparable to dirt or soil. For that reason, the airside exit stagnation temperature (T_{t5}), the exit water temperature (T_{wo}), and the overall heat transfer for a single bundle was calculated for a fouling layer thermal conductivity from 0.1 to 10 $W/m \cdot K$ [Hamdhan, 2010]. Utilizing empirical data recorded from five 16T tests in 2018, Table 4.1, for the inlet conditions, the results from Test 1 can be seen in Figures 4.1 - 4.3 below. In addition to the varying values of thermal conductivity, the effect of fouling layer thickness was also plotted for 50, 141, and 500μm thick fouling layers.

Table 4.1: 16T Test Conditions

	Test 1	Test 2	Test 3	Test 4	Test 5
M_1	0.83	0.65	1.05	1.5	1.6
T_{T1} [K]	314.54	318.37	319.93	311.59	311.09
P_{T1} [Pa]	119700	118637	71470	47880	48771
P_{T2} [Pa]	N/A	N/A	59672.8	32845.7	34109.7
T_{T4} [K]	335.15	338.48	343.15	355.43	352.32
T_{wi} [K]	294.87	299.82	299.82	294.26	285.71
$\dot{m}_w$ [kg/s]	6309.10	4037.82	6309.10	6309.10	1261.82

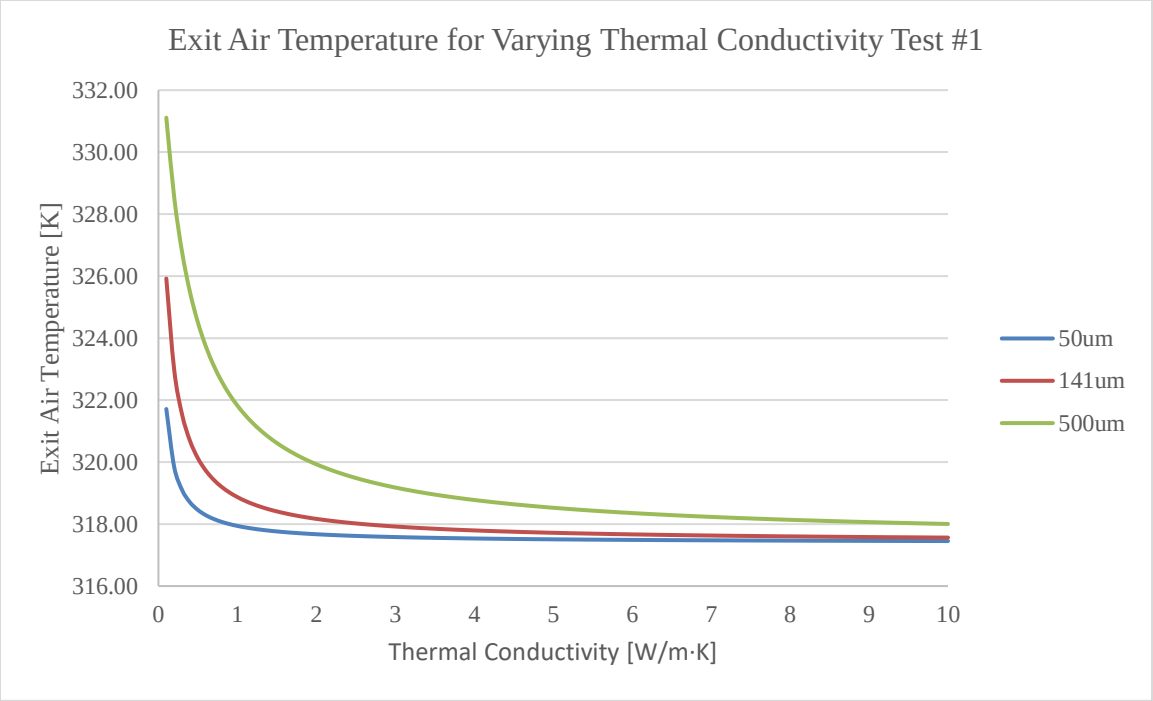


Figure 4.1: Exit Air Temperature for Varying Thermal Conductivity

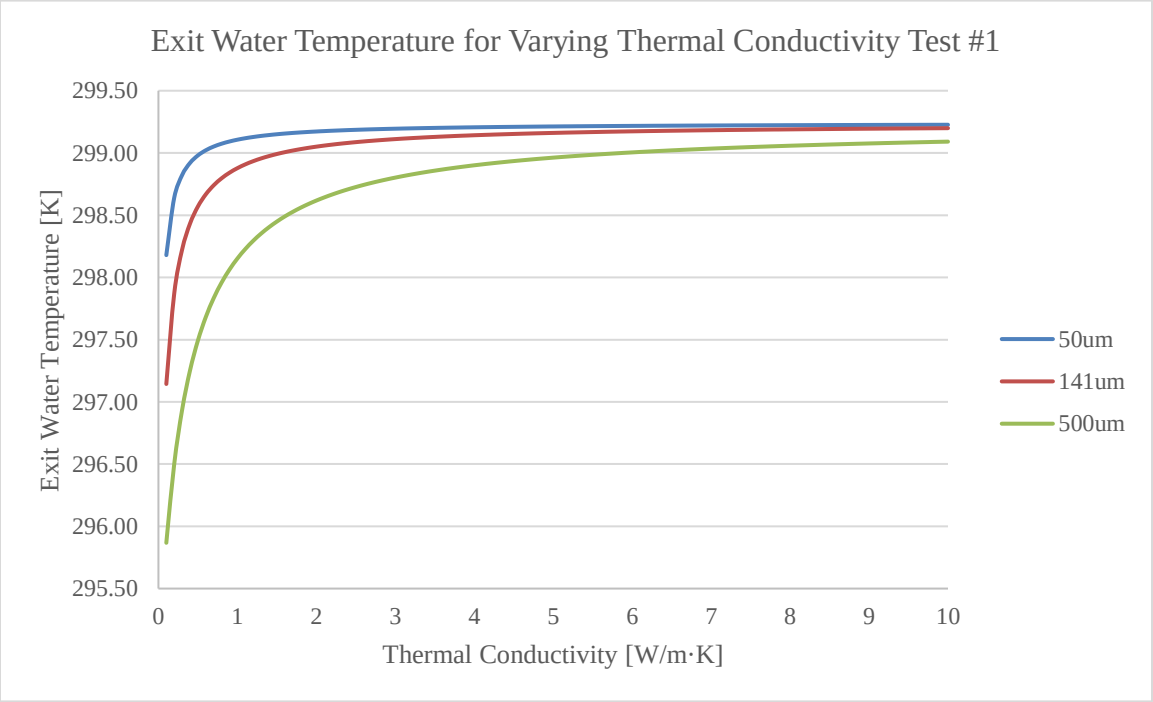


Figure 4.2: Exit Water Temperature for Varying Thermal Conductivity

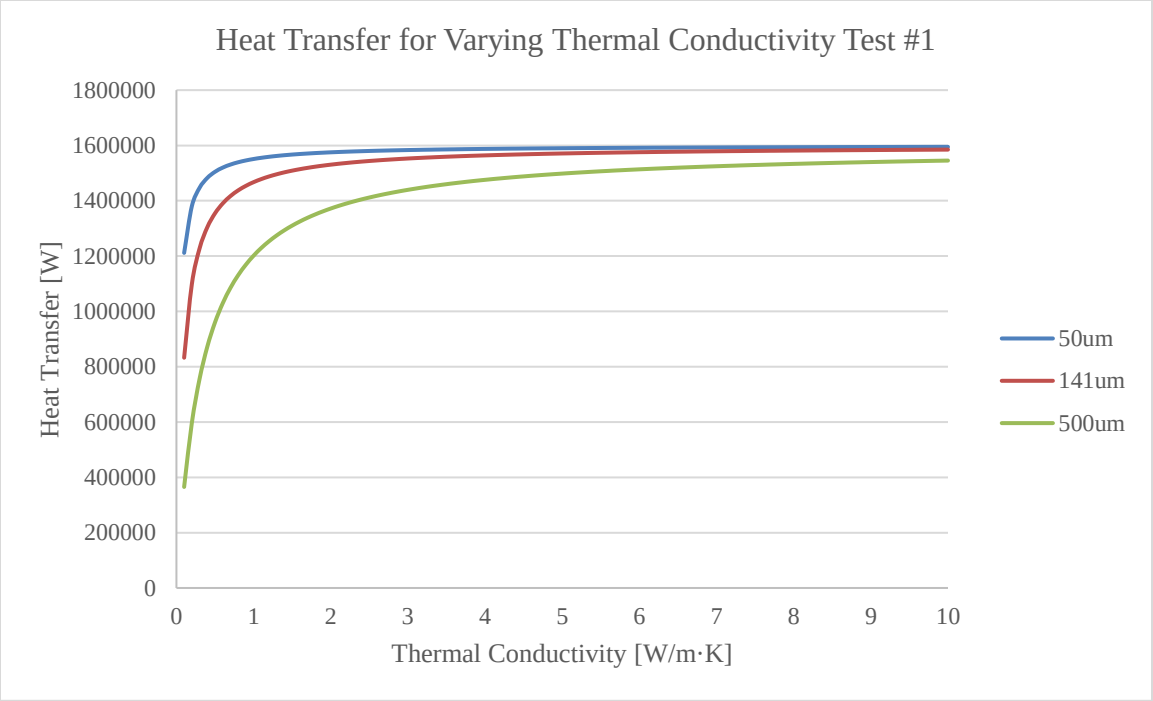


Figure 4.3: Heat Transfer for Varying Thermal Conductivity

Figures 4.1 - 4.3 illustrate that the magnitude of fouling layer thermal conductivity has a significant impact between zero and one. The curves approach an asymptote where the fouling layer thermal conductivity has a minimal effect on cooler performance. It should be noted that the thicker fouling layer (500μm in this case) allows for higher values of k_{foul} to affect cooler performance. This can be expected based on Equation 3.31. To contribute to cooler bundle performance, δ_{foul} must increase with k_{foul} or the value for fouling layer resistance will approach zero with an increased fouling layer thermal conductivity.

The exit air temperature is measured directly at the discharge of the cooler bundle (see Figure 3.1). As a result, the empirical data is more accurate for the discharge air temperature than the discharge water temperature: T_{t5} is measured per bundle, where T_{wo} is averaged for the entire cooler. The empirical data from all five test conditions were compared to the MATLAB simulation to determine a value for the fouling layer thermal conductivity that corresponded to the most accurate value for T_{t5}. The average value for fouling layer thickness (141 μm) was used to calculate the fouling layer thermal conductivity, k_{foul}. The average of all five tests was calculated (Table 4.2) and used for the fouling layer thickness analysis in the next section.

Table 4.2: Calculated Thermal Conductivity for Each Test

	Measured T_{t5} [K]	Calculated T_{t5} [K]	k_{foul} $[W/m \cdot K]$
Test #1	320.87	320.86	0.36
Test #2	325.43	325.42	0.27
Test #3	325.54	325.58	0.23
Test #4	324.65	324.63	0.22
Test #5	323.93	323.94	0.18
Average k_{foul}			**0.25**

Fouling Layer Thickness Analysis

With the average thermal conductivity known, the effects of fouling layer accumulation can be determined for a given value of k_{foul}. As stated in the problem statement, the overall goal of this study is to find how heat transfer performance is degraded over time. Design conditions were determined based on the 16T test cell operation envelope. The conditions assume a maximum test cell total pressure (P_{t1}) for Mach numbers (M_1) ranging from 0.6 to 1.6. Test section total temperature (T_{t1}) is assumed to be 310.93 K for all flow conditions. Inlet water temperature and water flow rate was assumed constant for all six conditions based on maximum K1 flow capabilities and highest expected inlet water temperature. See Table 4.3 for design conditions. Cooler inlet temperature and mass flow rate are the main contributing factors to the cooler performance. Both are a result of test cell requirements. Supersonic test cell conditions result in a higher cooler inlet temperature because of the increased power requirement from the compressor. Likewise, lower subsonic test conditions result in lower power requirements from the compressor. Alternatively, airside mass flow is the highest at subsonic conditions. Figures 4.4 - 4.8 show the comparison between the six test conditions (labeled based on test cell Mach Number) for $k_{foul} = 0.25$.

Table 4.3: Design Envelope for K1 Cooler

M_1	T_{T1} [K]	P_{T1} [Pa]	T_{T4} [K]	T_{wi} [K]	$\dot{m}_w$ [kg/s]	$\dot{m}_4$ [kg/s]
0.6	310.93	186732	329.26	302.59	6309.10	8704.70
0.8	310.93	153216	332.59	302.59	6309.10	8174.10
1.0	310.93	138852	334.26	302.59	6309.10	7690.90
1.2	310.93	114912	340.93	302.59	6309.10	6176.90
1.4	310.93	110124	347.59	302.59	6309.10	5471.00
1.6	310.93	100548	356.48	302.59	6309.10	4454.60

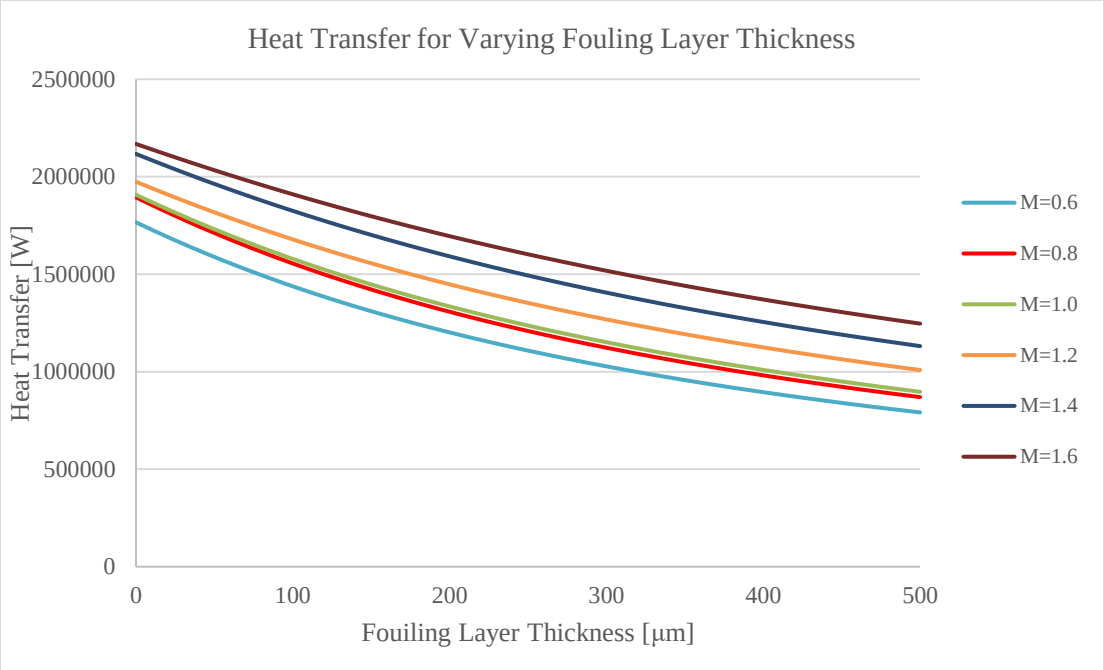


Figure 4.4: Heat Transfer for Varying Fouling Layer Thickness

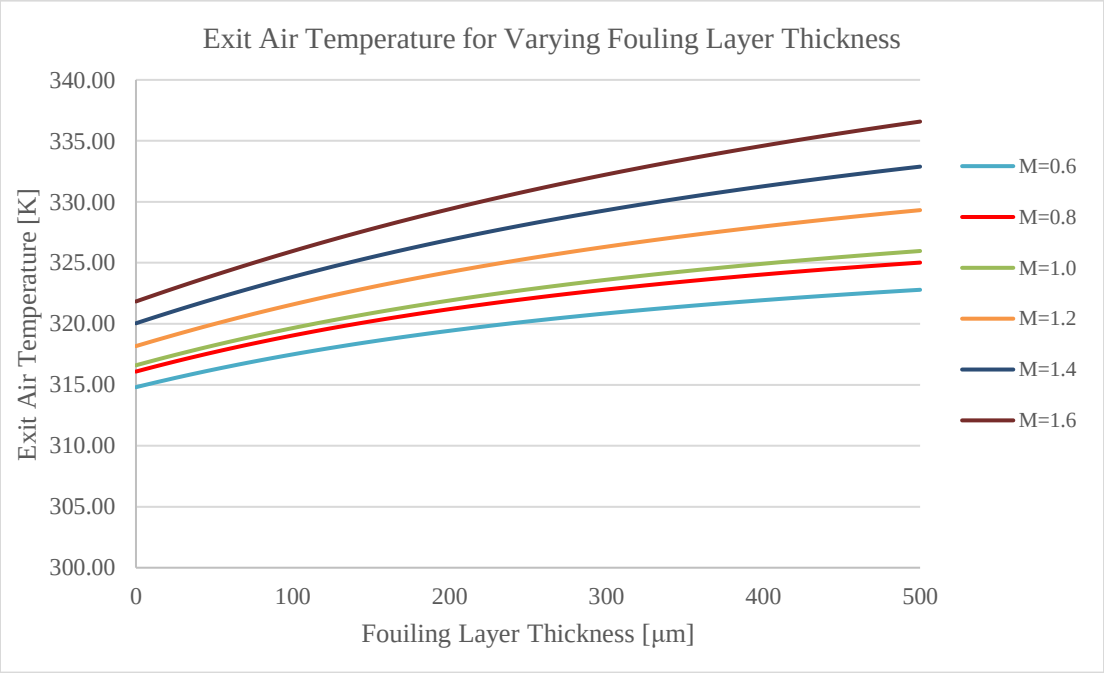


Figure 4.5: Exit Air Temperature for Varying Fouling Layer Thickness

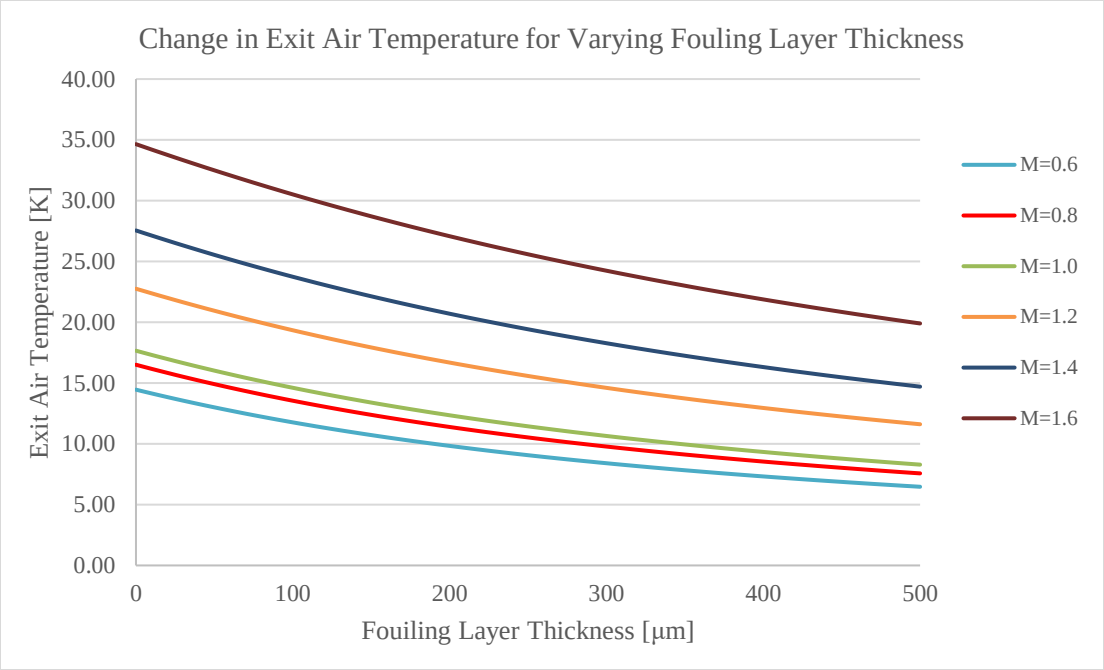


Figure 4.6: Air Temperature across Bundle for Varying Fouling Layer Thickness

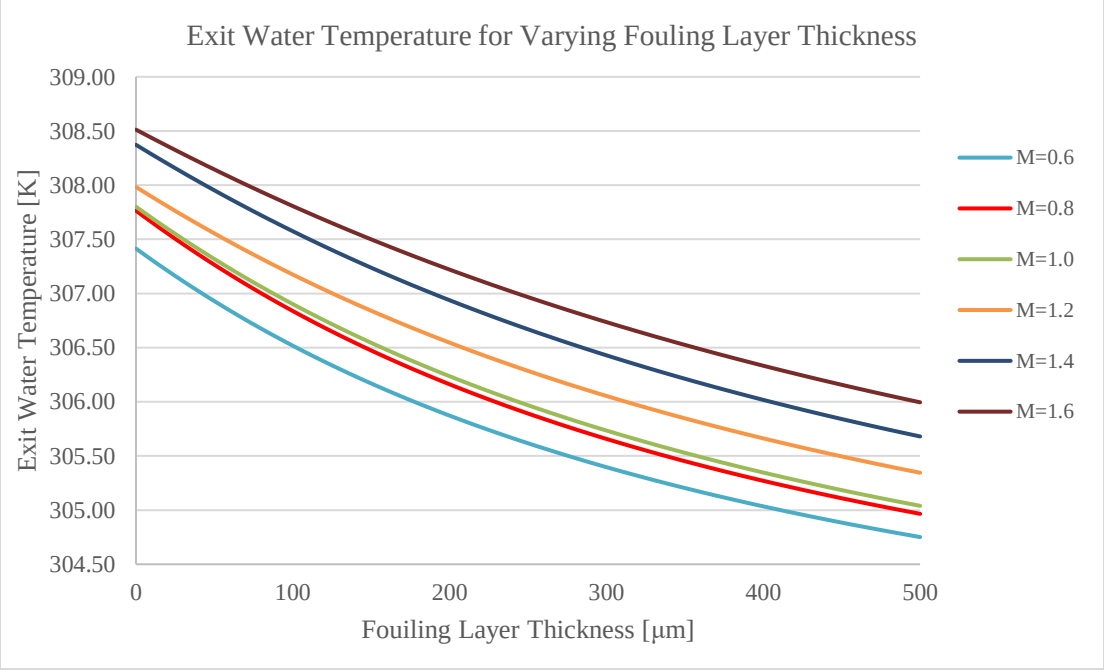


Figure 4.7: Exit Water Temperature for Varying Fouling Layer Thickness

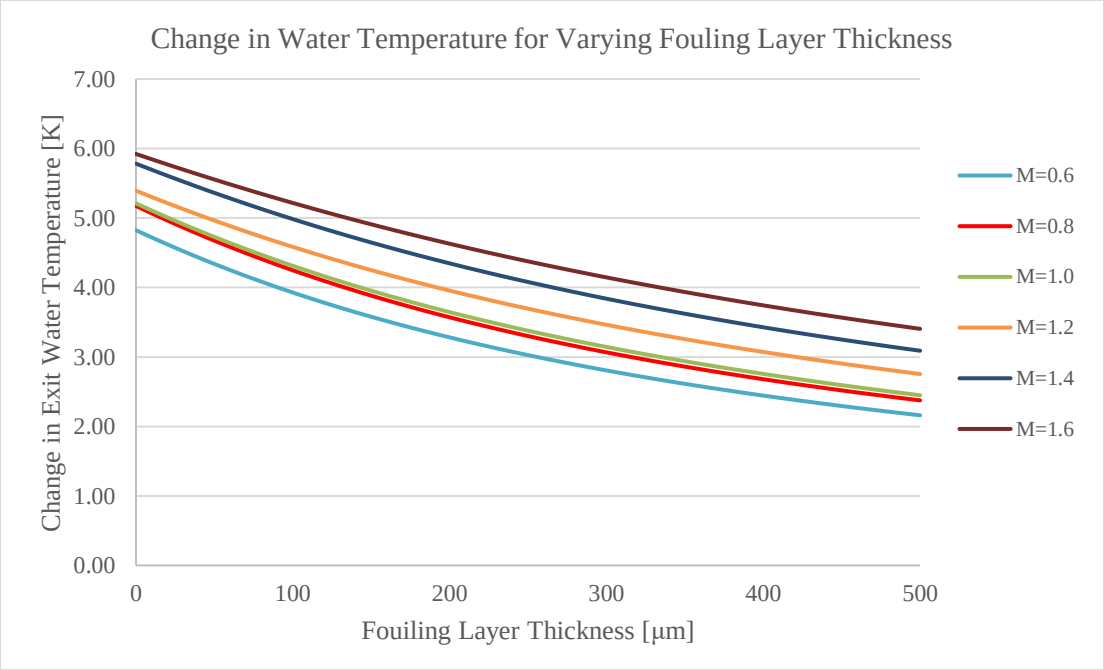


Figure 4.8: Water Temperature across Bundle for Varying Fouling Layer Thickness

Figures 4.4 - 4.8 prove that the overall effect of fouling layer thickness is significant across the entire 16T envelope. In addition, the impact on the performance parameters is comparable for all six test conditions. The difference in each parameter (heat transfer, air exit temperature, and water exit temperature) is a function of inlet conditions. $M_1 = 1.6$ results in the highest K1 inlet temperature (approx. 24 K higher than $M_1 = 0.6$) and puts the largest thermal requirement on the K1 cooler.

Source of Potential Error

The most likely source of errors is the fin and tube interface. This study assumes that the fin is completely attached the tube. In actuality, the fin is not attached but rather wrapped around the tube. The gap (regardless of how significant) would decrease the heat transfer capability of the bundle. It is expected that this study made up for this inefficiency in the calculation for the thermal conductivity of the fouling layer. The smaller the value for k_{foul}, the more inefficient the bundle. If the fin was fully attached to the tube, it is expected that the discharge temperatures would be lower, thus corresponding to a larger value of fouling layer thermal conductivity.

CHAPTER FIVE
CONCLUSIONS AND RECOMMENDATIONS

Based on the analysis and results presented above, this study answers the question as to how much additional heat capacity is required to account for age related fouling and degradation. Utilizing the same model that was developed in this study, the fouling resistance, R_f, can be calculated by Knudsen's equation [Awad, 2001] for fouling resistance. The calculated valve for fouling resistance for $M_1 = 1.6$ flow conditions can be seen in Table 5.1.

$$R_f = \frac{1}{U_f} - \frac{1}{U_c} \tag{5.1}$$

The fouling factor or fouling resistance in the original 1950s design of the K1 Cooler was $1.76x10^{-4}\ m^2K/W$ [Stacey Brothers Gas Construction Co., 1951]. After 17 years of operation, it can be seen in Table 5.1 that the initial assumption was too low.

In addition to fouling resistance, reduction in surface area from leaking tubes must also be a design consideration. The bundle selected for this particular study was installed in 2000 and operated for seventeen years before the tube sample was removed. To date, 41% of the heat transfer surface has been lost due to tube leaks. As previously stated, this can be caused by a number of reasons, but once a tube leaks, it is not repaired but instead abandoned. In addition to the effects of the fouling layer, an analysis was also completed to determine how much a reduced surface area affects overall cooler performance. To completely answer the original problem statement, the comparison must be made between "like new" and as found to determine the overall degradation of the cooler.

Utilizing the same model as described above, a comparison was made for $M_1 = 1.6$ between a bundle in "like new" condition and the bundle in its current condition seventeen years later. A third condition (assuming no loss in heat transfer surface area) was completed to emphasize the degrading effects of the 141μm thick fouling layer. These results are shown in Table 5.2.

Table 5.1: Fouling Resistance

U_C $[W/m^2K]$	U_f $[W/m^2K]$	R_f $[m^2K/W]$
117.81	83.13	0.0035

Table 5.2: Comparison between New Bundle and Current Bundle

	New Bundle	Fouled Bundle	Bundle Current Condition	Overall Difference
Years of Operation	0	N/A	17	17
δ_{foul} [µm]	0	141	141	141
% Tubes Cut	0	0	41	41
Heat Transfer [W]	2,150,038	1,805,057	1,267,598	882,441
Exit Air Temp. [K]	321.60	327.19	335.74	14.14
Exit Water Temp. [K]	308.46	307.52	306.08	2.41

While a 41% reduction in surface area in seventeen years is not the standard or average, there is the potential for it. And as seen in the table above, the impact of age-related degradation is not insignificant: a 41% decrease in heat transfer capability and a 14K increase in exit air temperature. This results in difficulties meeting test conditions and also increased test costs. Less capable cooling bundles require higher flow rates to meet the same test conditions. As a result, the customer is given a more expensive water bill.

The K1 Cooler bundles are currently being designed based on the 16T envelope for summer months (highest inlet water temperature). Since the new bundles are required to fit in the footprint of the existing bundle, this study recommends one of the two following options. Option 1 is to reduce the risk of future fouling and tube damage with additional systems such as filtration and water treatment. Option 2 is reducing the exit air design temperature by at least 4% to allow for any potential decrease in cooler performance from both fouling layer accumulation and loss of tubes as the system ages. This would ensure that the cooler would continue to make test conditions as the performance degrades as well as provide the added benefit of lower cooling water requirements while the bundle is still new. While it is expected that a trade study be completed weighing the benefits and cost/challenges of each option, both provide a viable option to for the K1 Cooler to successfully support 16T testing for many years.

LIST OF REFERENCES

Anderson, John D. *Modern Compressible Flow with Historical Perspective*. 3rd ed., McGraw-Hill, 2004.

Awad, Mostafa M. (January 28th 2011). Fouling of Heat Transfer Surfaces, Heat Transfer, Aziz Belmiloudi, IntechOpen, DOI: 10.5772/13696. Available from: https://www.intechopen.com/books/heat-transfer-theoretical-analysis-experimental-investigations-and-industrial-systems/fouling-of-heat-transfer-surface

Bejan, Adrian. *Convective Heat Transfer*. 4th ed., John Wiley & Sons, Inc., 2013.

Hamdhan, Indra Noer. "Determination of Thermal Conductivity of Coarse and Fine Sand Soils" *Proceedings World Geothermal Congress*, 2010. International Geothermal Association, https://www.geothermal-energy.org/pdf/IGAstandard/WGC/2010/2952.pdf

Ibrahim, Hassan Al-Haj. (September 26th 2012). Fouling in Heat Exchangers, MATLAB, Vasilios N. Katsikis, IntechOpen, DOI: 10.5772/46462. Available from: https://www.intechopen.com/books/matlab-a-fundamental-tool-for-scientific-computing-and-engineering-applications-volume-3/fouling-in-heat-exchangers

Kazi, S. N. (March 9th 2012). Fouling and Fouling Mitigation on Heat Exchanger Surfaces, Heat Exchangers, Jovan Mitrovic, IntechOpen, DOI: 10.5772/32990. Available from: https://www.intechopen.com/books/heat-exchangers-basics-design-applications/heat-exchanger-fouling-and-its-mitigation

Lee, HoSung. (2013). Compact Heat Exchangers. [online] Western Michigan University. Available at: http://homepages.wmich.edu/~leehs/ME539/Chapter%205%20HSL.pdf

Test Facilities Handbook. 13th ed., Arnold Engineering Development Center, 1992.

The Stacey Bros. Gas Construction Co. "Process Design Report Covering Heat Transfer Surface Cooler No. 1." *Design Report No. DR-1*, 6 July 1951.

Wais, Piotr. "Fin-Tube Heat Exchanger Optimization." *Heat Exchangers - Basics Design Application*s, 2012. IntechOpen, www.intechopen.com/books/heat-exchangers-basics-design-applications/fin-tube-heat-exchanger-optimization-.

VITA

Derrick Alan Talley was born March 1992 in Birmingham, AL. After graduating from Hewitt-Trussville High School in 2010, he attended The University of Alabama from 2010 to 2014 and received his Bachelor of Science degree in Aerospace Engineering. Derrick accepted a position as a Mechanical Systems Engineer for Aerospace Testing Alliance at Arnold AFB in 2014 working at the Propulsion Wind Tunnel. He is currently a Test Operations Engineer for the Space and Missiles Test Group for National Aerospace Solutions at Arnold AFB. He continued his education to obtain his Master of Science degree in Mechanical Engineering from the University of Tennessee. In the future, he plans to obtain his Professional Engineering license and continue his work as a Test Operations Engineer.